*Russian Chemical Reviews* **76** (5) 415 – 433 (2007) © 2007 Russian Academy of Sciences and Turpion Ltd

DOI 10.1070/RC2007v076n05ABEH003687

# Ionics of nanoheterogeneous materials

N F Uvarov

## Contents


| | | |
|---|---|---|
| I. | Introduction | 415 |
| II. | General criteria for the choice of composite electrolytes with high ionic conductivity | 416 |
| III. | Surface disordering of ionic crystals | 417 |
| IV. | Disordering of ionic crystals at interfaces. Conductivity of microcomposites | 420 |
| V. | Calculations of physicochemical properties of composites | 421 |
| VI. | Thermodynamic description of composites. The effect of self-dispersion of ionic salts. Synthesis of nanocomposites | 423 |
| VII. | Size effects in composites | 424 |
| VIII. | Conclusion | 430 |


**Abstract. The results of studies of composite ionic conductors are considered. The relationship between their properties and the ionic salt disordering and the interfacial interaction between the components of the material is analysed. Special attention is paid to models that describe the surface disordering and the mechanism of defect formation. The methods of calculation of physicochemical characteristics of composites, the thermodynamic stability and peculiarities of the genesis of the nanocomposite morphology are discussed. The bibliography includes 188 references.**

## I. Introduction

Ionics, *i.e.*, a science that studies ionic processes in systems and materials, is a comparatively new and rapidly progressing field of knowledge.[1–3] Although it ranks much below electronics in the practical application, its role tends to increase. This is caused first of all by the demands for new and more efficient electrochemical systems for the accumulation and conversion of energy at a constant threat of the shortage of natural energy resources. This problem can be solved given a wide spectrum of electrolytes with different functional characteristics that can be adapted to the specific conditions of operation of various electrochemical systems. Solid electrolytes that exhibit high mechanical strength, thermal stability, unipolar ionic conductivity and can be used in chemical power sources, gas sensors and other electrochemical devices occupy a special place among these electrolytes.

Heterogeneous doping of ionic compounds with dispersed dielectrics that are chemically inert with respect to the ionic salt is known to enhance the conductivity in most cases. Composite solid electrolytes of the ionic salt – oxide (MX – A) type can be considered as a new class of ionic conductors with high ionic conductivity. The combination of high conductivity with the enhanced mechanical strength together with the wide prospects for the targeted modification of the electrolyte properties by varying the type and concentration of the dopant makes these composites promising materials for real electrochemical systems. The composites $LiI - Al_2O_3$ synthesised by Liang in 1973 proved to be convenient solid electrolytes for chemical power sources.[4, 5] This achievement has triggered a scientific boom, and a large number of composite ionic conductors were studied in the subsequent years. Actually, doping with dispersed oxides was shown to enhance the conductivity of virtually all composites based on classical (non-superionic) ionic salts, *i.e.*, it is a general effect, which requires scientific explanation and theoretical substantiation.

There are several reviews devoted to the description and the analysis of the ion transport in polycrystalline and composite solid electrolytes.[6–22] The increase in the ionic conductivity upon heterogeneous doping can be explained within the framework of the space charge model proposed by Wagner and Maier,[6, 7, 9, 10, 12, 13, 15] which represents a version of the classical Frenkel's model.[23] This model allows the interpretation of many phenomena observed in composites and is the best suited for the explanation of experimental data for composites containing oxides with relatively coarse grains. However, the space charge model in its classical version is correct only for ideal crystals in contact with vacuum or a structure-free medium and obviously ignores the real features of the interphase contact, namely, changes in the structures of ionic crystals (*e.g.*, for epitaxial contacts), the effect of elastic strains, the formation of dislocations, *etc.* Moreover, if the surface concentration of defects is sufficiently high, it is impossible to ignore the interaction between the defects, which results in their ordering and the formation of superstructures and even metastable surface phases.

It is known that the conductivity of composites increases as the size of dopant particles increases. Hence, composites with nanosized grains (about 10 nm) are of particular interest for practice. Obviously, uniform mixing of such an oxide with an ionic component should produce a nanocomposite the properties of which strongly depend on the energy of surface interaction and the peculiarities of the interface between the phases. For composites with coarse-grained dopants, the presence of surfaces or interphase contacts has virtually no effect on the bulk properties of the ionic salt; hence, the

**N F Uvarov** Institute of Solid State Chemistry and Mechanochemistry, Siberian Branch of the Russian Academy of Sciences, ul. Kutateladze 18, 630090 Novosibirsk, Russian Federation. Fax (7-383) 332 28 47, tel. (7-383) 332 56 45, e-mail: uvarov@solid.nsk.su

Received 11 December 2006
*Uspekhi Khimii* **76** (5) 454 – 473 (2007); translated by T Ya Safonova

increase in the conductivity is of the purely surface nature. However, in many cases, it still remains unclear whether the enhanced conductivity is primarily caused by the specific interactions at the interface or by the trivial increase in the surface conductivity as such. To answer this question, information on the conductivity of polycrystals is necessary. In nanocomposites, an ionic salt is virtually totally located at the interface. This is why its structure and thermodynamic characteristics can substantially change. Particularly, for ionic compounds containing high-temperature disordered phases, the latter may prove to be stable at low temperatures in nanocomposites. Therefore, it is important to understand the thermodynamic reasons for the appearance of a disordered phase. To this end, it is necessary to elucidate how the thermodynamic parameters of crystals, particularly, the enthalpy and entropy of phase transitions are related to the lattice disorder.

In this review, the problems of thermodynamic stability of nanocomposites and the genesis of the composite morphology during its sintering are discussed; possible mechanisms of the interfacial interaction and the general trends for the changes in the ionic salt properties are analysed for a wide series of ionic salt – oxide systems; size effects and methods for the quantitative estimation of conductivity and other physicochemical characteristics of composites are considered.

## II. General criteria for the choice of composite electrolytes with high ionic conductivity

Even in their first stage, the studies have revealed the following relationships typical of the composite solid electrolytes MX – A:[6–8, 10–15]

— due to heterogeneous doping, a region of low-temperature conductivity with a lower activation energy ($E_a$) appears in the Arrhenius plots of conductivity in addition to the region of intrinsic conductivity (at high temperatures);

— in the low-temperature region, the concentration dependence of the conductivity has a maximum at a dopant concentration of 10 vol.% – 40 vol.%; in certain systems, the maximum is observed at lower dopant concentrations (1 vol.% – 10 vol.%);

— in the high-temperature region, the conductivity monotonously decreases with the increase in the dopant concentration; an analogous effect is observed in superionic phases;

— the conductivity of composites usually increases with the decrease in the size ($L_A$) of particles of the heterogeneous dopant or with the increase in its specific surface ($S_A$).

All composite solid electrolytes known can arbitrarily be divided into two groups:[24]

(1) Composites MX – A with the properties similar to those of polycrystals MX (*e.g.*, $LiI-Al_2O_3$, $AgCl-Al_2O_3$, $AgBr-Al_2O_3$ and $TlCl-Al_2O_3$). In this case, the activation energy of the composite MX – A is close to $E_a$ of polycrystalline MX and virtually coincides with the enthalpy of migration of a cationic vacancy ($E_{cv}$) in the single crystal MX. This is an argument for the applicability of the space charge model for the explanation of the conductivity mechanism in composites.[6–8, 10, 12–15]

(2) Composites with unusual properties. In certain composites, the physicochemical properties of ionic salts substantially differ from those of single-crystal and polycrystalline samples. The activation energy often substantially depends on the type and concentration of a fine-grain dopant and may far deviate from both $E_{cv}$ and $E_a$. In certain cases, the observed deviations were apparently due to the insufficiently wide temperature ranges in which the conductivity was measured. However, the specific interaction between the composite components can also be a reason for the dramatic changes in the $E_a$ values. For example, in composites $AgI-Al_2O_3$, the temperature of the β-AgI phase transition into the superionic state was observed to decrease, which was accompanied by a decrease in the enthalpy of the phase transition.[25,26] For composites $AgI-Fe_2O_3$ both the changes in the parameters of the AgI phase transition and the increase in the Néel temperature for $Fe_2O_3$ were observed.[27] This suggests that the thermodynamic parameters of both bulk phases are different in composites. In certain composites, in addition to the conventional phases, new phases non-typical of pure ionic crystals were revealed.

These facts suggest that the interfacial interaction in composites may substantially affect the bulk physicochemical properties of the ionic component in a composite. However, so far, no systematic studies were carried out aimed at the synthesis of composites and the investigation of anomalous properties of the constituent ionic salts. The majority of studies were focused on the increase in the ionic conductivity. The theoretical models that describe the increase in the ionic conductivity are usually tested on quite different objects that usually exhibit no high conductivity.

Insofar as the thermodynamic parameters of ionic salts in composites can substantially change, it is important to study their relationship with the surface disordering. The deeper insight into the mechanism and thermodynamic peculiarities of the formation of defects in the crystal bulk, on its surface or on intergrain boundaries requires the knowledge of how the point defects affect the thermodynamic properties of crystals. One may consider the inverse problem, namely, judge on the degree of disordering of a solid based on the analysis of the thermodynamic data. The most distinct changes in vibrational spectra and the degree of disordering occur during the phase transitions and give rise to easily measurable changes in the entropy and enthalpy of a crystal. The presence of grain and phase boundaries affects the concentration of defects in a crystal and can lead to changes in the thermodynamic parameters of phase transitions. Thus, it is expected that the thermodynamic studies of phase transitions would provide information on the disordering of the ionic component in a composite.

In contrast to crystals in which the self-diffusion coefficients may differ by several orders of magnitude, the transport properties of melts are approximately the same for all substances. In this respect, the molten state is universal, most disordered, and the thermodynamic parameters of melting (or crystallisation) contain information on the degree of disordering of a crystal at the melting temperature. Hence, it is the correlations between the parameters of melting and the transport properties of solids that attract the prime interest. Elucidation of the factors responsible for melting allows one to get a clearer insight into the processes that occur in the transition of a substance into the superionic or orientationally disordered state in both pure crystals and ionic salts brought in contact with the surface of another phase.

It was shown[28–33] that for a wide range of substances a linear correlation is observed between the enthalpy of melting ($H_{melt}$) and the enthalpy of formation of Schottky defects ($h_0$) (Fig. 1)

$$h_0 = \beta H_{melt}. \quad (1)$$

The ratio $h_0/H_{melt} = \beta = 8.6 \pm 0.6$ is independent of the type of the substance and remains unchanged in binary ionic substances, metals and molecular crystals. In contrast to the correlations such as $h_0 = aT_{mp}$, which are cited most often but are fulfilled for a limited range of substances, correlation (1) is more general. Within the framework of the phenomenological quasicrystalline model, the melting process can be presented as an abrupt increase in the mole fraction of point defects in a crystal ($c$) up to a certain critical value $c_L$ followed by the relaxation of the structure around defects. In this approximation, the parameter $\beta$ has a simple physical meaning and is defined as $\beta = 1/c_L$. The constancy of $c_L = 0.12 \pm 0.02$ for

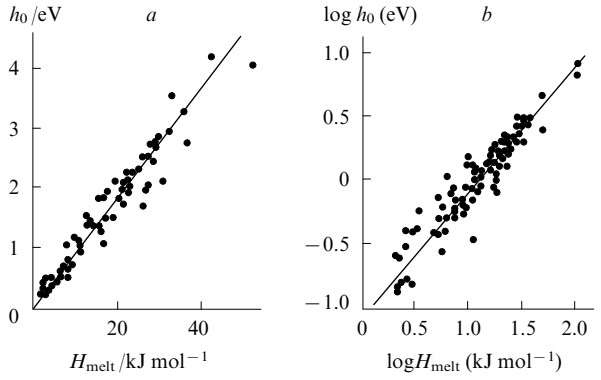



**Figure 1.** Correlation between the enthalpy of melting ($H_{melt}$) and the enthalpy of formation ($h_0$) of the Schottky defects in crystals presented in (*a*) linear and (*b*) logarithmic scales.

substances with different types of interatomic interactions may be assumed as a characteristic feature of the liquid state. The relative changes in the volume upon melting ($\Delta V/V$) are associated with the volume of the defect formation $v_0$ ($\Omega$ is the molecular volume)

$$\frac{\Delta V}{V} = c_L \frac{v_0}{\Omega}.$$

This relationship was confirmed experimentally for metals and crystalline alkali metal halides (in this case, $v_0$ is the volume of formation of the Schottky defect).[33] Melting with the formation of the Schottky defects or the vacancy melting is always accompanied by an increase in the volume. Some substances ($H_2O$, Bi, Sb, Si, Ge, $RbNO_3$) melt with a decrease in their volumes. In this case, the melting apparently follows the inerstitial mechanism, *i.e.*, involves the formation of Frenkel defects, the volume of formation of which (in contrast to the Schottky defects) can be negative.

If we assume that the vibrational frequencies of atoms or ions in a liquid are equal to those of atoms around a defect in a crystal, it is possible to assess the entropy of the defect formation ($s_0$) and the concentration of defects in crystals at the melting temperature ($c_{mp}$). The calculated $s_0$ and $c_{mp}$ values agree sufficiently well with experimental data for metals and ionic crystals.[34,35] Insofar as for metals and alkali metal halides, a linear correlation is observed between the enthalpy of defect formation and the enthalpy of migration, one can estimate the absolute magnitudes of the coefficients of self-diffusion or ionic conduction based on $H_{melt}$.[28–30,36] The correlations mentioned can be found in the well-known reference book.[37]

Superionic conductors form an unusual class of ionic conductors characterised by the high conductivity comparable with that of ionic melts and aqueous solutions. The equilibrium concentration of current carriers in superionic conductors is high and comparable with the total amount of mobile ions in the lattice, *i.e.*, $h_0$ is close to zero. Superionic conductors and ionic melts are known to exhibit common features, for example,

— a diffuse distribution of the ion density along the conduction channels, which is analogous to the broad radial distribution function of the same ions in melts;

— close values of ionic conductivity and, hence, only minor changes in the conductivity in the melting;

— substantial changes in the thermodynamic parameters of substances upon their transition into the superionic state, which are comparable in the magnitude with the corresponding effects in the melting.

High-temperature phases of AgI and $Li_2SO_4$ are typical examples of superionic conductors. On the qualitative level, a superionic conductor may be represented as a partly ordered system built of two sublattices, one of which is entirely ordered and forms a rigid frame and the other is strongly disordered and resembles a liquid phase that fills the frame. The expressions for the melting temperature, which were derived within the framework of the quasicrystalline model of melting are similar to those obtained by Gurevich for a 'strong' superionic transition.[38–40] This similarity forms the basis for the prediction (if only on the qualitative level) of certain properties of superionic conductors. Apparently, the assumption that $c \approx 1$ is not true for superionic conductors. By analogy with melts, it can be expected that $c \approx c_L = 0.12$. Because no reliable methods were developed so far for the estimation of the defect concentration in superionic conductors, it remains unclear what is the concentration of defects in superionic phases.

An interesting class of ionic conductors is formed by the phases that contain orientationally disordered anions. Obviously, the orientational disordering should entail an increase in the free volume in crystals, which will favour the increase in the diffusion coefficients and in the ionic conductivity. Moreover, the of anion reorientation event may additionally facilitate the transfer of the neighbouring cation by the 'paddle-wheel' mechanism proposed by Lunden.[41] The thermodynamic parameters of phase transitions are related to the extent of the crystal disorder at a temperature below the phase transition. This relationship manifests itself most clearly in a series of alkali metal nitrates for which a decrease in the enthalpy and entropy of melting is accompanied by an increase in the conductivity of high-temperature phases.[24,42] Alkali metal nitrates form an unusual class of inorganic salts, being characterised by phase transitions with orientational disordering in the anionic sublattice.[43] Among the nitrates, rubidium nitrate has the lowest $H_{melt}$ and demonstrates three phase transitions associated with the orientational disordering of $NO_3^-$ ions.[42] The thermodynamic data correlate well with the ionic conductivity, *i.e.*, rubidium nitrate exhibits the highest ionic conductivity in the series of nitrates[42] and is promising for the development of ionic conductors with the high rubidium conductivity.[44] This is why, in this review, attention is focused on rubidium nitrate and composites on its basis.

In composites and, particularly, nanocomposites, the interfacial interaction affects the energy of an ionic crystal thus favouring the stabilisation of high-temperature disordered phases. The phase-transition temperature and enthalpy may serve as the convenient parameters that characterise the degree of disordering and the changes in the energy characteristics of a crystal in a composite. For this reason, compounds containing high-temperature superionic or orientationally disordered phases were chosen as the best candidates for the ionic salt component in the ionic salt – oxide composites.

## III. Surface disordering of ionic crystals

Embarking on the discussion of the effect of heterophase additives, it is necessary to consider the possible mechanisms of disordering, *i.e.*, the formation of point defects on the free surface of an ionic crystal. In is known that in many cases the conductivity of polycrystalline samples exceeds that of single crystals. Hence, simple dispersion of an ionic crystal MX may be one of the reasons for the increase in its conductivity in composites. This is accompanied by the formation of a large number of free surfaces or grain boundaries MX – MX, which are characterised by the enhanced surface or intergrain conductivity. As a rule, the increase in the concentration of surface defects is associated with the formation of an electrical double layer in the near-surface region of a crystal.

Currently, the interpretation of surface phenomena in ionic crystals widely employs the Frenkel – Kliewer model.[23, 45–48] This model was first proposed by Frenkel [23] and is based on the assumption that different types of defects can form separately and independently in the crystal bulk due to the difference in their chemical potentials. Frenkel assumed this to be associated with the appearance of an electrical potential in the crystal bulk, which may be considered as a contact potential drop in the crystal surface layer, caused by the difference in the energies of formation of positive and negative defects that appear on the surface.[23] Figure 2 *a* illustrates the changes (in terms of the Frenkel model) in the energy parameters, the defect concentration and the electrical potential on going from the ionic crystal surface to its bulk. This model was analysed most comprehensively in the studies by Kliewer.[47, 48]

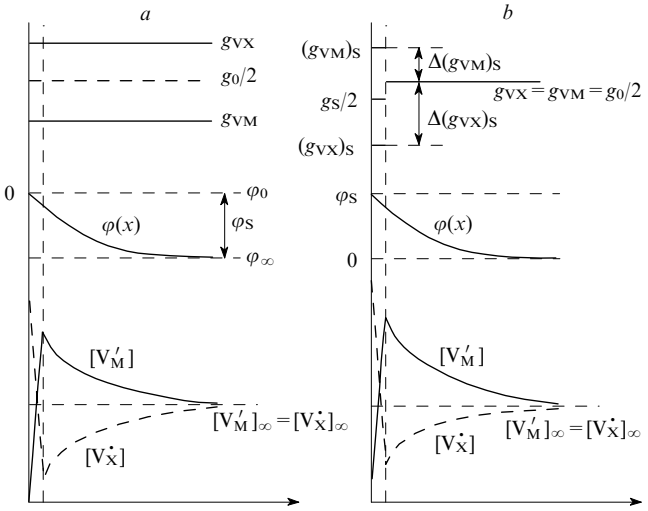



**Figure 2.** Changes in the energy parameters ($g$), potential ($\varphi$) and defect concentration ([V]) on going from the surface to the bulk of an ionic crystal.
(*a*) The Frenkel model; the surface potential $\varphi_S$ is equal to the potential difference between the surface ($\varphi_0$) and the bulk ($\varphi_\infty$) of a crystal; (*b*) the Stern model; a case of a diffuse layer enriched with cationic vacancies is considered.

According to this model, the surface potential $\varphi_S$, *i.e.*, the potential difference between the surface and the bulk of an ionic crystal MX containing intrinsic Schottky defects is

$$e\varphi_S = \frac{g_{VX} - g_{VM}}{2}, \qquad (2)$$

where $e$ is the electron charge, $g_{VX}$ and $g_{VM}$ are the partial energies of the formation of anionic and cationic vacancies in the crystal bulk the sum of which is equal to the energy of formation ($g_0$) of the Schottky defect. This expression is remarkable because it contains no characteristics directly related to the surface properties, namely, the quantities $g_{VM}$ and $g_{VX}$ (as well as $g_0$) are the bulk parameters of the substance; hence, the quantity $\varphi_S$ should be a universal constant of a given substance. However, it is well known that the real surface properties are determined by several specific factors such as the crystal plane type, defects, adsorbed impurities, *etc.*, which casts doubt on the validity of the Frenkel – Kliewer model.

The surface potential can be calculated using a more realistic Stern model,[49] which implies that the physical properties of a crystal and all its components (native and foreign ions, point defects) on the surface differ from those in the bulk. Particularly, the energies of formation of individual defects on the surface $(g_{VX})_S$, $(g_{VM})_S$ and the energy of the proper surface disordering $g_S = (g_{VX})_S + (g_{VM})_S$ will differ from the corresponding parameters in the crystal bulk. This difference is the reason for the adsorption (positive or negative) of defects on the crystal surface. If the adsorption energies of oppositely charged defects differ, the excessive defects with the most negative adsorption energies are concentrated on the surface, while the opposite-sign defects form a diffuse layer under the surface. Figure 2 *b* shows the corresponding energy diagram and the distribution of defects in a crystal. According to the Stern model, the surface charge ($Q_S$) is defined as a sum of contributions of different defects each calculated based on the Langmuir isotherm

$$Q_S = N_S \sum_i q_i \left[1 + \frac{1}{x_i} \exp\left(\frac{\Delta g_i - q_i \varphi_S}{kT}\right)\right]^{-1},$$

where $N_S$ is the concentration of accessible surface sites (adsorption centres), $q_i$ is the effective charge of defects, $x_i$ is the mole fraction of defects in the crystal bulk, $\Delta g_i$ is the adsorption energy of the $i$th defects (*i.e.*, the excess Gibbs energy of a crystal due to the transition of a defect of the $i$th kind from the crystal bulk to the surface), $k$ is the Boltzmann constant, $T$ is the absolute temperature; summation is carried out over all possible charged defects. The surface charge is compensated by the charge ($Q_d$) of a diffuse layer, which is formed under the crystal surface and described by the Gouy – Chapman equation for the diffuse layer charge

$$Q_d = A\left\{\sum_i N_{0i} x_i \left[exp\left(-\frac{q_i \varphi_{S-1}}{kT}\right) - 1\right]\right\}^{1/2},$$

where $A = (2\varepsilon\varepsilon_0 kT)^{1/2}$, $\varepsilon$ is the dielectric permittivity, $\varepsilon_0$ is the dielectric constant; $N_{0i}$ is the bulk concentration of the $i$th ions in the crystal; $\varphi_{S-1}$ is the potential of the outer Helmholtz plane. The assumption that the surface charges are equal to the diffuse layer charge allows one to obtain a transcendental equation the solution of which gives the surface potential.

The analysis of solutions of this equation [50] showed that the form of the dependence $\varphi_S(T)$ is entirely determined by the values of $\Delta g_i$, $g_0$ and $N_S$. For positive adsorption energies ($\Delta g^- > 0$, $\Delta g^+ > 0$, negative adsorption), the defect concentration on the crystal surface is lower than in its bulk. In this case, the surface charge and potential are close to zero. For negative adsorption energies of defects ($\Delta g^- < 0$, $\Delta g^+ < 0$, positive adsorption), the cationic and anionic vacancies are concentrated on the surface to form a negative (at $|\Delta g^-| > |\Delta g^+|$) or positive (at $|\Delta g^-| < |\Delta g^+|$) surface charge. Figure 3 shows the dependences of the surface potential on the temperature for a crystal of the NaCl type with the Schottky defects, which were calculated for fixed parameters $g_0 = 1.0$ eV, $\Delta g^- = -0.1$ eV and different values of $\Delta g^+$ ($\Delta g^+ < 0$). The analysis has shown that the form of $\varphi_S(T)$ curves changes as follows depending on the ratio between $g_0$ and $\Delta g^+$:

1. For small energies of defect adsorption ($|\Delta g^+| < g_0/4$; $\Delta g^+ < 0$), the quantity $\varphi_S(T)$ increases monotonically with the temperature; at $T \to 0$, $\varphi_S \to 0$ (Fig. 3 *a*). Such a behaviour of the surface potential cannot be explained within the framework of the Frenkel – Kliewer model [48, 49] and is described by the following approximate formula obtained [50] for the case of the low potentials $e\varphi_S/kT \ll 1$:

$$\varphi_S \approx \frac{2kT}{AN_0} N_S \left[\exp\left(-\frac{\Delta g^+}{kT}\right) - \exp\left(-\frac{\Delta g^-}{kT}\right)\right] \times \qquad (3)$$

$$\times \sqrt{N_0} \exp\left(-\frac{g_0}{4kT}\right).$$

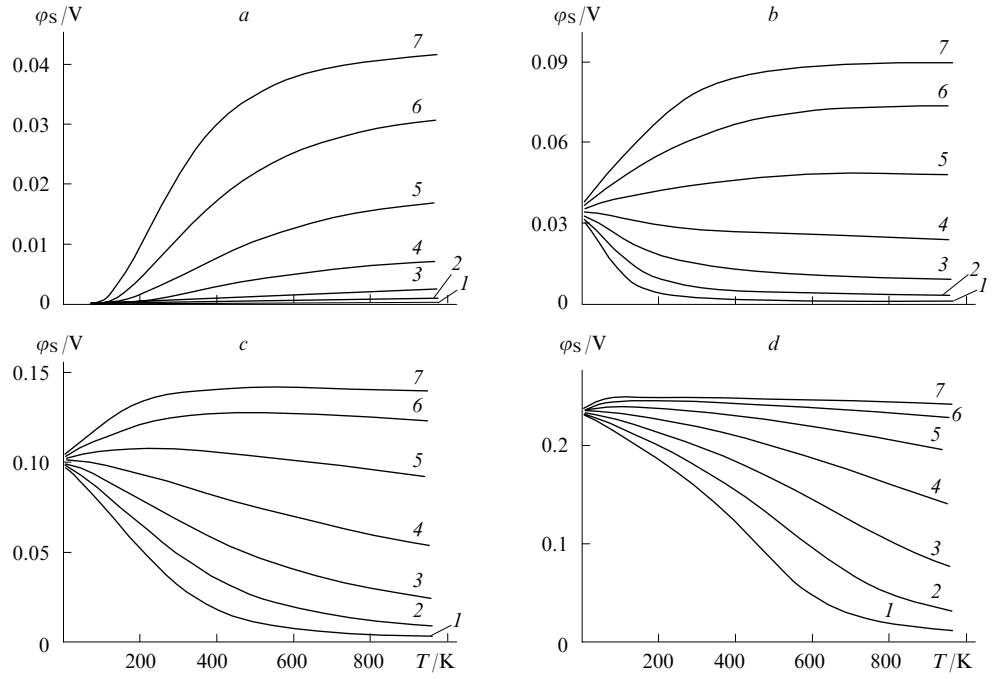



**Figure 3.** Temperature dependences of the surface potential calculated in terms of the Stern model for $g_0 = 1.0$ eV, $\Delta g^- = -0.1$ eV and $\Delta g^+ = -0.2$ (*a*), $-0.3$ (*b*), $-0.4$ (*c*) and $-0.6$ eV (*d*).
Concentration of surface sites ($N_S$) is (cm$^{-2}$): (*1*) $1 \times 10^{12}$, (*2*) $3 \times 10^{12}$, (*3*) $1 \times 10^{13}$, (*4*) $3 \times 10^{13}$, (*5*) $1 \times 10^{14}$ (*6*) $3 \times 10^{14}$ and (*7*) $1 \times 10^{15}$.

This equation is identical to the expression derived by Lifshits and Geguzin.[51] According to Eqn (3), the surface potential is determined not only by the difference between $\Delta g^+$ and $\Delta g^-$ but also by the energy of defect formation. The quantity $\varphi_S$ increases with the increase in the concentration of surface sites in proportion to the square root of the Schottky defect concentration in a crystal. Thus, for a low adsorption energy, the formation of a double layer is limited not only by the number of surface sites but also by the capacity of the crystal to form a diffuse layer, *i.e.*, by the density of bulk defects.

2. For high adsorption energies ($|\Delta g^+| > g_0/4$; $\Delta g^+ < 0$), the shape of $\varphi_S(T)$ curves substantially changes (Fig. 3 *b*–*d*). In the limit at $T \to 0$, the dependence $\varphi_S(T)$ tends not to zero but to a certain value $\varphi_S^*$ determined by the relationship

$$e\varphi_S^* = \frac{2}{3}\left(-\Delta g^+ - \frac{g_0}{4}\right).$$

In the general case, the surface potential can either increase or decrease depending on the quantities $\Delta g^+$ and $N_S$. For very high adsorption energies $|\Delta g^+|$, the temperature dependences $\varphi_S(T)$ differ insignificantly from the curves obtained within the framework of the Poeppel – Blakely model,[52] which makes an attempt to take into account the effect of the limited number of accessible surface sites on the surface potential. This case is shown in Fig. 3 *d*, namely, at small $N_S$, the number of surface sites becomes the limiting factor and the surface potential falls to zero with the increase in the temperature, whereas at large $N_S \sim 10^{15}$ cm$^{-2}$, the function $\varphi_S(T)$ tends to the high-temperature limit determined by the equation

$$\varphi_S = \frac{\Delta g^- - \Delta g^+}{2e}. \qquad (4)$$

A comparison of expressions (4) and (2) shows that they are identical under the assumption that

$$\Delta g^- - \Delta g^+ = (\Delta g_{VM})_S - (\Delta g_{VX})_S = g_{VX} - g_{VM}.$$

Thus, for sufficiently high $|\Delta g^+|$ and $N_S$ values and after the renormalisation of the energy values, the Stern model leads to the same result as the Frenkel – Kliewer and Poeppel – Blakely models.

The Stern model allows one to calculate the surface potential in different types of ionic crystals. In the general case, the calculated parameters of this model include the energy of defect formation, the energy of adsorption of defects and impurity ions, the concentration of surface sites, the concentration of impurities and the temperature. This model allows one to calculate $\varphi_S$ in NaCl crystals containing admixed bivalent metals and to assess the isoelectric temperature. The Stern model can be used for the interpretation of experimental $\varphi_S$ values for AgCl and AgBr and also for the calculation of the surface defect concentration in a model superionic oxygen conductor $M^{4+}_{1-c}M^{3+}_c O_{2-0.5c}$. The main advantages of the Stern model are that all its parameters have clear physical meaning, its solution can be found relatively simply and it can be applied to a wide range of problems that include the investigation of segregation effects and the interaction of defects on interfaces.

In the first approximation, the conductivity of a real polycrystalline specimen can be described in terms of a model of cubic blocks by the following expression:[9, 53]

$$\sigma \approx 2\sigma_\perp(4\sigma_\parallel + \sigma_b)(2\sigma_\perp + \sigma_b)^{-1},$$

where $\sigma_\perp$ and $\sigma_\parallel$ are the contributions of double layers oriented normally and in parallel to the electric field, respectively, to the conductivity; $\sigma_b$ is the conductivity in the crystal bulk. Usually, for crystals $\sigma_\perp \gg \sigma_\parallel$, and the conductivity of a specimen is determined by the sum of bulk and surface conductivities. If the same carriers are responsible for the conductivity in the crystal bulk and in the diffuse layer, the conductivity of a polycrystal is expressed by the equation

$$\sigma = \sigma_b\left[1 + \frac{8\lambda_D}{L}\exp\left(\pm\frac{e\varphi_S}{2kT}\right)\right] \quad (5)$$

and is determined by the effective layer thickness equal to the double Debye length of screening ($2\lambda_D$), the block size ($L$) and the surface potential. The Debye length depends on the concentration of carriers in the crystal bulk and, in the general case, on the temperature. It was shown that the activation energy of conduction of an impurity-free MX crystal is

$$E_a = \frac{h_0}{4} - \frac{e\varphi_S}{2} + E_m, \quad (6)$$

*i.e.*, it is determined by the bulk characteristics of the solid, namely, the enthalpies of formation ($h_0$) and migration ($E_m$) of a defect and the surface potential ($\varphi_S$).

Studies of polycrystalline AgCl have shown [24] that the conductivity of specimens non-subjected to long-term annealing is determined by the conductivity of intergrain boundaries. The estimates of the surface potential based on relationship (6) produce quite reasonable values $\varphi_S = 0.1-0.2$ V, provided the conductivity is assigned to interstitial cations that form the diffuse layer. Polycrystalline specimens demonstrated the dielectric relaxation with a small increment $\Delta\varepsilon/\varepsilon_0 \approx 3$. On annealing, the activation energy of conduction was observed to increase monotonically and the quantity $\Delta\varepsilon/\varepsilon_0$ vanished.

Studies of polycrystalline AgI have shown [54–56] that the conductivity of mechanically dispersed samples far exceeds the conductivities of β- and γ-phases of AgI cited in the literature. Upon heating or storage at room temperature, the conductivity decreased, which was accompanied by a gradual increase in the activation energy of conduction from 0.23 to 0.31 eV. For specially purified specimens, the Arrhenius plots demonstrated a bend at a temperature $T_b$ in the range from 0 to 40 °C. After sintering at $T > 150$ °C, the absolute magnitudes of conductivity virtually coincided with that of a β-AgI single crystal. The static permittivity ($\varepsilon_s$), which does not depend on the electrode polarisation, substantially increased to $\varepsilon_s/\varepsilon_0 \sim 50-200$ after the specimens were pressed or mechanically treated, whereas the high-frequency permittivity ($\varepsilon_\infty$) ($\varepsilon_\infty/\varepsilon_0 = 8 \pm 2$) was close to the permittivity of pure β-AgI. The observed changes can be explained by the formation of β–γ-polytypes containing randomly alternating closely packed layers (in contrast to the regular packing ABABAB or ABCABCABC in the β- and γ-phases, respectively). Insofar as the unit cells in both phases (in both γ-AgI and β-AgI) possess no inversion centres, the mechanical activation of polytypes can shift the closely packed layers. This is accompanied by changes in the polar axis direction and may result in the formation of a contact between two layers $I^- - Ag^+$. The cations on two sides of the contact plane are in different tetrahedral positions. This contact represents an antiphase boundary, *i.e.*, a boundary between antiphase domains. In this case, the strong Coulomb interaction between the $Ag^+(T_+)$ and $Ag^+(T_-)$ layers is compensated by the partial transition of $Ag^+$ ions from their regular positions to the vacant tetrahedral and octahedral positions, *i.e.*, to form the Frenkel defects at the antiphase boundary. The accumulation of the space charge at antiphase boundaries is the reason for the high dielectric permittivity of this material.

The presence of a small concentration of a heterogenic admixture (*e.g.*, metallic silver) stabilises the antiphase domains. A qualitatively similar effect was observed in the AgI – poly(tetrafluoroethylene) system.[57,58] The mechanism of stabilisation of antiphase boundaries resembles that of dispersion strengthening in metals where fine heterogeneous inclusions prevent the annealing of grain boundaries.

## IV. Disordering of ionic crystals at interfaces. Conductivity of microcomposites

The physical reason for the surface interaction in a composite of the ionic salt – oxide type lies in the trend of both substances to decrease their surface energy due to the interaction of surface ions with the ions of the neighbouring phase. The surface energy of the interface between an ionic salt MX and alumina is determined in the first approximation as a sum of the cation – cation ($M^+ - Al^{3+}$), cation – anion ($Al^{3+} - X^-$ and $M^+ - O^{2-}$) and anion – anion ($X^- - O^{2-}$) interactions ($E_{M-Al}$, $E_{X-Al}$, $E_{M-O}$ and $E_{X-O}$, respectively)

$$G^s_{MX-A} = \gamma_{MX-A}S_{MX-A} \approx E_{M-Al} + E_{Al-X} + E_{M-O} + E_{X-O},$$

where $\gamma$ is the specific surface energy and $S$ is the surface area.

For the sake of simplicity, we assume that, as a result of their interaction, the lattices of MX and A phases are fitted to one another at the interface. Because the energies $E_{M-Al}$, $E_{X-Al}$, $E_{M-O}$ and $E_{X-O}$ are different in the magnitude (due to the different energies of interaction in the ion pairs $M^+ - Al^{3+}$, $Al^{3+} - X^-$, $M^+ - O^{2-}$ and $X^- - O^{2-}$), in the interface layers, the ideal structure inherent in individual phases will be distorted in such a way as to provide a gain in the surface energy due to the mutual approach or removal of surface atoms. The relative displacement of ions from their ideal positions is determined by the balance of energies $E_i$. Insofar as in alumina and in majority of salts MX under discussion, anions exceed cations in size, it can be expected that for close packing, the interface cations will have the larger free volumes and be displaced by longer distances than anions. As a result, in the space between the surface layers, an intermediate positively charged layer enriched with cations is formed, the charge of this layer being compensated by the cationic vacancies $(V'_M)_S$ that constitute the diffuse layer. The process of structural relaxation can be presented as the following quasichemical reaction:

$$0 \rightleftharpoons V'_M + (M-A)^{\cdot}_S, \quad (7)$$

which describes the stage of the surface disordering of MX at the MX – A interface (the superscripts $^{\cdot}$ and $'$ correspond to the positive and negative charges of a species, respectively, as compared with the stoichiometric charge of a given lattice site). If an anion is adsorbed on the surface, another reaction proceeds

$$0 \rightleftharpoons V^{\cdot}_X + (X-A)'_S. \quad (8)$$

The isoelectric point of an oxide p$E$ was proposed [59] as a measure of its surface activity. Indeed, equations similar to Eqns (7) and (8) may be written for the surface interaction of an oxide with water

$$H_2O \rightleftharpoons OH' + (H-A)^{\cdot}_S, \quad (9)$$
$$2H_2O \rightleftharpoons H_3O^{\cdot} + (OH-A)'_S.$$

The first reaction predominates for oxides with p$E > 7$, for instance $Al_2O_3$, $CeO_2$; the second prevails for oxides with p$E < 7$ ($ZrO_2$, $SiO_2$). By analogy with aqueous solutions, one can expect that the surface reaction (7) will occur in composites containing basic oxides (p$E > 7$), whereas for acidic oxides (p$E < 7$) the interface interaction will follow the mechanism (8). Unfortunately, to date, due to the insufficient amount of experimental data, it is difficult to check the correctness of the direct transfer of the model of acid – base equilibria in aqueous solutions to the case of composites. Nonetheless, the competition between processes (7) and (9)

$$V'_M + (M-A)^{\cdot}_S + H_2O \rightleftharpoons OH' + (H-A)'_S + MX$$

can be responsible for the deterioration of the ionic conductivity of composites $AgCl-Al_2O_3$ (Ref. 60) and $AgI-Al_2O_3$ (Ref. 61) and the appearance of the protonic conductivity in composites $Li_2SO_4-Al_2O_3$ (Ref. 62) and $M(NO_3)_n-Al_2O_3$ (M is an alkali metal) [63] in humid atmosphere.

In essence, reactions (7) and (8) describe the formation of the electrical double layer on the surface of MX in contact with $Al_2O_3$. The changes in the energy ($\Delta g_A$) upon the displacement of an ion from its normal position into the interfacial space can be considered as the energy of cation adsorption in terms of the Stern model; hence, the quantity $\Delta g_A$ is related to the surface potential ($\varphi_{SA}$) at the interface of a crystal MX

$$\varphi_{SA} \sim -\frac{\Delta g_A}{q_i}, \qquad (10)$$

where $q_i$ is the charge of the displaced ion. Insofar as the exact $\varphi_{SA}$ value is determined not only by the quantity $\Delta g_A$ but also by the contribution of the relaxation of oxide ions, expression (10) can be considered as merely a correlation between the values $\Delta g_A$ and $\varphi_{SA}$, *viz.*, the surface potential increases with the increase in $\Delta g_A$. For $T = 0$ K, on the surface of a salt MX in contact with an oxide, a dense layer similar to the Helmholtz layer exists. With the increase in the temperature, the cationic vacancies form a diffuse layer, which provides the enhanced conductivity of the composite.

Insofar as ions in the dense layer are bound to the surface of oxide A and have limited mobility, the conductivity of MX in composites is determined by the defects that dominate in the diffuse layer. The mobility of defects in the diffuse layer is assumed equal to their mobility in the crystal bulk.[6, 7, 10, 12, 13, 15] This statement is based on the assumption that the defect concentration in the surface layer remains low; hence, the crystal structure does not change (the absence of deformations, surface phase transitions, *etc.*). Within the framework of these assumptions, the conductivity across the diffuse layer in the composite is described by expression (5), where $\varphi_{SA}$ should be substituted for $\varphi_S$ and the migration energy $E_m$ pertains to the defects that form the diffuse layer. For low $\varphi_{SA}$, *i.e.*, for a relatively weak surface interaction, the absolute magnitudes of conductivity are low and the activation energy of conduction is

$$E_a = \frac{h_0}{4} - \frac{e\varphi_{SA}}{2} + E_m.$$

The quantity $E_a$ can vary within the limits $(h_0/4 + E_m) > E_a > (h_0/4 + E_m - e\varphi_{SA}/2)$ and is sensitive to the surface state of the MX–A contact, *i.e.*, to the presence of structural defects, adsorbed admixtures, *etc.*; the measured parameters of conductivity are often characterised by poor reproducibility. Such effects are observed in insufficiently sintered composites.

If as a result of surface interaction, the surface potential increases to its limiting value $e\varphi_S = h_0/2$, the activation energy of conduction decreases to $E_a = E_m$ [see Eqn (6)]. As was shown by Maier,[10, 13, 15] the activation energy of conduction in composites MX–A is close to the energy of migration of a cationic vacancy, which indirectly confirms the fact that the surface potential is sufficiently high and reaction (7) proceeds on the interface to afford a diffuse layer built of cationic vacancies.

Most composites considered in the early studies can be classified with microcomposites, because they were prepared from oxides with the average particle size of 0.06–10 μm. The properties of microcomposites are similar to those of polycrystalline specimens, and all physicochemical properties of ionic salts (except for the ionic conductivity) in these systems are analogous to the properties of pure starting compounds. A typical example of such systems is the composites $AgCl-Al_2O_3$. The dependence of the conductivity ($\sigma$) on the mole fraction ($x$) of the oxide has a maximum at $x = 0.30$, the activation energy of conduction is close to the energy of migration of cationic vacancies.[6, 60] The estimates of the energy of formation of silver chloride in a composite, which were obtained using an electrochemical cell $Pb/PbCl_2/(1-x)\,AgCl-x\,Al_2O_3/Ag$, showed that the thermodynamic properties of AgCl in composites remain virtually unchanged.[64] The exposure of composites to a humid medium lead to the reduction of their conductivity, particularly, at $x > 0.5-0.6$.[60]

Based on correlations obtained earlier [65, 66] and an assumption that $E_a = E_m$, it is possible to assess the concentration of current carriers in composites. The following relationship between the conductivity at 25 °C ($\sigma_{25}$/S cm$^{-1}$), the defect concentration ($n$/cm$^{-3}$) and the activation energy ($E_a$/eV) was proposed:[53]

$$\log \sigma_{25} = \log n - 14.5\,E_a - 20.55.$$

In composites with the highest conductivity, the concentration of defects proved to be high and comparable with their concentration in superionics. This suggests that additional channels for the defect formation exist in composites so that the correct interpretation of experimental data requires that the specifics of interphase interactions and the real structure of the interface were taken into account. It cannot be ruled out that the disordered surface phases formed at the interface will manifest most strongly their specific properties on going from micro- to nanocomposites. These effects are discussed below.

## V. Calculations of physicochemical properties of composites

The model of cubic blocks,[53, 67] which is similar to that used earlier to describe the conductivity of polycystalline specimens, may be applied for the quantitative calculation of the physical characteristics of composites MX–A. If a layer with a thickness $\lambda$ and properties differing from those of the MX phase in the substance bulk exists near the interface, this layer can be conditionally assumed to be the surface phase. The model of cubic blocks allows one to estimate the volume and mole fractions of the surface phase ($f_S$ and $x_S$, respectively) for the uniform random distribution of equal-size particles MX and A in a composite

$$f_S = \frac{2\beta\lambda f(1-f)}{L_A},$$

$$x_S = \frac{2\beta\lambda\delta x(1-x)}{L_A[1 + x(\delta - 1)]},$$

where $\beta$ is the constant determined by the particle geometry, for cubic or spherical particles, $\beta \approx 3$; $\lambda$ is the surface phase thickness; $f$ and $L_A$ are the volume fraction and the size of particles of the component A in the composite; the coefficient $\delta$ is determined by the ratio of densities ($d$) and molecular masses ($\mu$) of components, namely, $\delta = (\mu_A d_{MX})/(\mu_{MX} d_A)$; $x$ is the mole fraction of the component A. The volume fraction of an ionic salt $(f_{MX})_{bulk}$ beyond the surface layer can be determined using the expression

$$(f_{MX})_{bulk} = 1 - f - f_S = \left[1 - \frac{2\beta f\lambda}{L_A}\right](1-f),\ (f_{MX})_{bulk} \geqslant 0, \qquad (11)$$

which is very convenient for the estimation of the surface layer thickness provided the size of particles A is known. In real systems, $L_A$ corresponds to the size of an aggregate of particles A and $d_A$ corresponds to the average density of aggregates.

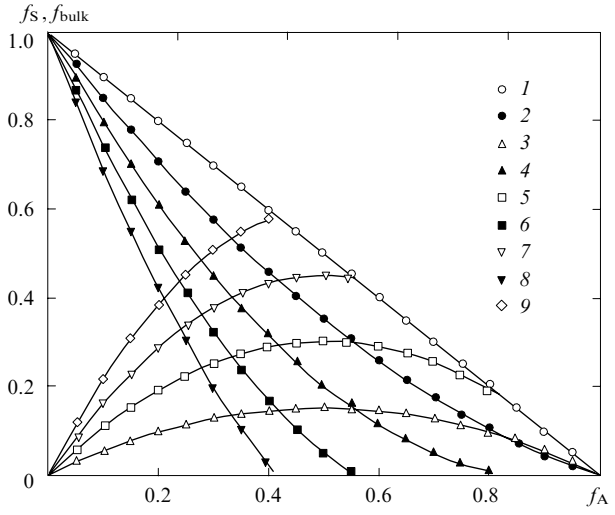



**Figure 4.** Concentration dependences of (*1*, *2*, *4*, *6*, *8*) bulk ($f_{bulk}$) and (*3*, *5*, *7*, *9*) surface ($f_S$) phases in composites calculated based on the model of cubic blocks for different ratios $\lambda/L_A$.
$\lambda/L_A = 0$ (*1*), 0.1 (*2*, *3*), 0.2 (*4*, *5*), 0.3 (*6*, *7*), 0.4 (*8*, *9*).

Expression (11) allows one to determine the ratio $\lambda/L_A$ based on the concentration dependence of any extensive characteristic of the MX phase; moreover, provided the average size of A particles is known, the absolute magnitude of the surface phase thickness $\lambda$ can be found (Fig. 4).

To assess the conductivity of composites, the models of effective medium or the theories of percolation, which were adapted to the specific features of the morphology of composites, are used. The most precise calculations of the conductivity of conventional composites of the conductor–dielectric type $(1-f)M-fA$ can be performed for the limiting cases ($f \to 0$ and $f \to 1$), where the particles of phases A or M pertain to the second-phase matrix and are isolated from one another. As the volume fraction of the second phase increases, its particles are no longer isolated and the calculations of the conductivity of composites require the use of more intricate models. A simpler method for the calculation of the composite conductivity based on the well-known mixing equation was proposed [68, 69]

$$\sigma^{\alpha} = (1-f)\sigma_M^{\alpha} + f\sigma_A^{\alpha}, \qquad (12)$$

where the parameter $\alpha$ is determined by the empirical fitting of dependence (12) to experimental values. The comparison of Eqn (12) with the exact solutions obtained for the limiting cases showed that the parameter $\alpha$ depends on the composite morphology. The morphology of real composites changes as the content of the second component increases, which makes extremely difficult the theoretical calculations of the conductivity within the framework of models mentioned above. The use of rules of mixing allows one to solve this problem by introducing the linear dependence of the power index $\alpha$ in Eqn (12)

$$\alpha \equiv \alpha(f) = \alpha_1(1-f) + \alpha_2 f, \qquad (13)$$

where $\alpha_1$ and $\alpha_2$ are the constants corresponding to the morphology of composites in the regions of limiting dilution (for $f \to 0$ and $f \to 1$, respectively). Taking into account expression (13), it is possible to represent expression (12) in the general form

$$\sigma^{\alpha_1(1-f)+\alpha_2 f} = (1-f)\sigma_M^{\alpha_1(1-f)+\alpha_2 f} + f\sigma_A^{\alpha_1(1-f)+\alpha_2 f}. \qquad (14)$$

In the limiting cases, Eqn (14) is reduced to expressions obtained within the framework of the effective medium model. The form of dependences $\log\sigma(f)$ and $\sigma(f)$ shown in Figs 5 *a*,*b* is entirely determined by $\alpha_1$ and $\alpha_2$. These dependences allow one to describe the conductivity of composites the morphology of which is determined by quite different factors including the percolation effect. The theoretical curves are close to those obtained using the McLachlan equation,[70] which is widely employed for the description of the percolation behaviour of composites. Figure 5 *c* shows the experimental conductivity of different composites [71] in comparison with calculated curves.

As in the case of conductor–dielectric composites, the most accurate calculations of the conductivity of solid electrolytes $(1-f)MX-fA$ can be performed for the limiting cases ($f \to 0$ and $f \to 1$), where isolated particles of phases A or MX are located in the second phase matrix. In the general case, the conductivity of model systems is described in terms of a percolation model [11] with two percolation thresholds, namely, $p_1$ (dielectric MX–ionic conductor) and $p_2$ (ionic conductor–dielectric A). The most serious difficulties in calculations

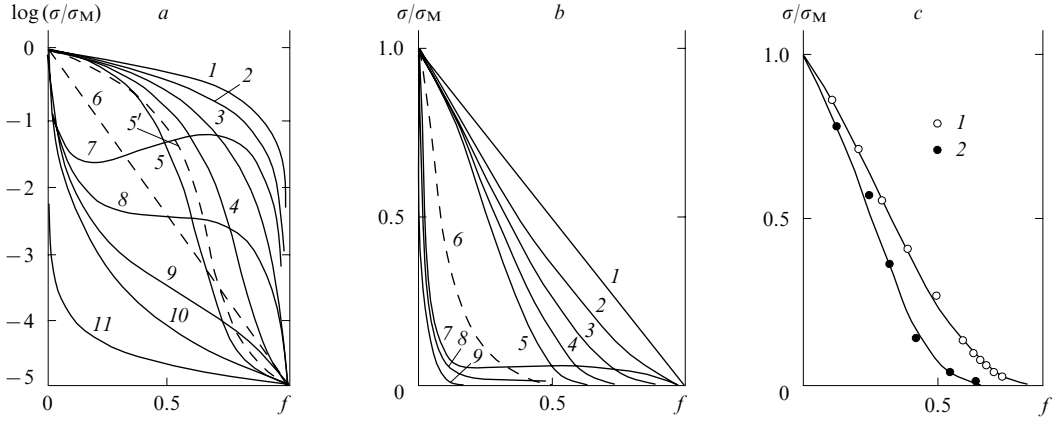



**Figure 5.** Calculated dependences of the relative conductivity ($\sigma/\sigma_M$) of composites MX–A on the bulk concentration of dielectric ($f$), shown in (*a*) logarithmic and (*b*) linear scales and (*c*) their comparison with experimental conductivity of composites AgI–$Al_2O_3$ (*1*) [61] and AgI–poly(tetrafluoroethylene) (*2*).[57, 58]
The curves were obtained for different ($\alpha_1$, $\alpha_2$): (*1*) (1, 1), (*2*) (2/3, 2/3), (*3*) (2/3, 1/3), (*4*) (2/3, 0), (*5*) (2/3, −1/3), (*6*) (0, 0), (*7*) (−1/3, 2/3), (*8*) (−1/3, 1/3), (*9*) (−1/3, 0), (*10*) (−1/3, −1/3), (*11*) (−1, −1); curve (*5′*) was calculated using the McLachlan equation.[70]

emerge in the vicinity of percolation thresholds at $f \approx p_1$ or $p_2$. In these regions, intricate models [72–81] are used. Moreover, even for composites with simple morphologies, rather cumbersome analytical expressions with a large number of fitting parameters should be used, which complicates the testing and practical application of these models. The mixing equation can be applied for the description of composite ionic conductors. The additional contribution of the surface conductivity can be taken into account in terms of the model of cubic blocks, which allows one to assess the concentration of the surface conducting phase. The mixing equation should take into account the contribution of this phase and can be presented as follows:

$$\sigma^{\alpha} = \left[1 - f - 6f(1-f)\frac{\lambda}{L_A}\right]\sigma_M^{\alpha} + 6f(1-f)\sigma_S^{\alpha}\left(\frac{\lambda}{L_A}\right) + f\sigma_A^{\alpha}. \quad (15)$$

For $6(\lambda/L_A)\sigma_S \gg \sigma_{MX}$, the expression takes a simpler form

$$\sigma = \left[6f(1-f)\frac{\lambda}{L_A}\right]^{1/\alpha}\sigma_S. \quad (16)$$

For $\alpha > 0$, dependence (16) has a symmetrical form with the maximum at $f = 0.5$. The introduction of the linear dependence $\alpha = \alpha(f)$ [expression (15)], which takes into account the changes in the morphology, allows one to obtain a modified mixing equation suitable for the description of conductivity of composite solid electrolytes. Analysis showed that the form of curves substantially depends on the parameters $\alpha_1$, $\alpha_2$ and that theoretical curves allow one to describe the conductivity as a function of the composition for specimens with totally different morphologies (Figs 6 *a*,*b*). It is interesting that the conductivity of a composite should increase with the increase in the size of particles of the oxide additive according to the exponential law $\sigma \sim (1/L_A)^{\beta}$, where $\beta = \alpha^{-1} \geqslant 1$, and only in the limiting case $\alpha(f) = 1$, it is expressed by the relationship $\sigma \sim (1/L_A)$ conventionally used in the literature.[15, 22, 25, 26]

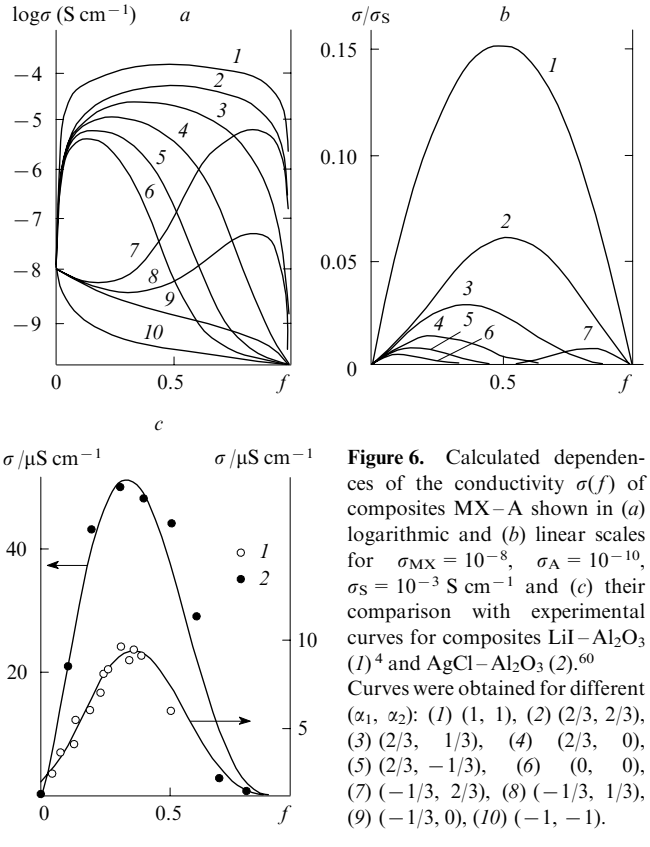



**Figure 6.** Calculated dependences of the conductivity $\sigma(f)$ of composites MX–A shown in (*a*) logarithmic and (*b*) linear scales for $\sigma_{MX} = 10^{-8}$, $\sigma_A = 10^{-10}$, $\sigma_S = 10^{-3}$ S cm$^{-1}$ and (*c*) their comparison with experimental curves for composites LiI–$Al_2O_3$ (*1*)[4] and AgCl–$Al_2O_3$ (*2*).[60] Curves were obtained for different ($\alpha_1$, $\alpha_2$): (*1*) (1, 1), (*2*) (2/3, 2/3), (*3*) (2/3, 1/3), (*4*) (2/3, 0), (*5*) (2/3, −1/3), (*6*) (0, 0), (*7*) (−1/3, 2/3), (*8*) (−1/3, 1/3), (*9*) (−1/3, 0), (*10*) (−1, −1).

Equation (15) type describe well the experimental data for composites LiI–$Al_2O_3$ (Ref. 4) and AgCl–$Al_2O_3$ (Ref. 60) (Fig. 6 *c*). The mixing equation in the form (15) is qualitatively consistent with the basic expressions obtained within the framework of the effective medium model and the percolation theory and also with the results of computer calculations.

## VI. Thermodynamic description of composites. The effect of self-dispersion of ionic salts. Synthesis of nanocomposites

In the general case, a solid-phase composite represents a complex multicomponent system that comprises several real solid phases. By a real solid phase is meant a combination of single crystals of different sizes, which contain admixtures, lattice defects (point defects and pores), free surfaces, cracks and grain boundaries. Many properties of composites depend on their morphology, *viz*., the size distributions of particles of each phase and the mutual spatial arrangement of monophase domains. In the presence of the surface interaction between the phases MX and A, the expression for the excess Gibbs energy of the composite can be presented as follows:[24, 82–84]

$$G = (G_{MX}^{\circ} + \gamma_{MX}S_{MX} + \Delta G_{MX}^{elas}) + \quad (17)$$
$$+ (G_A^{\circ} + \gamma_A S_A + \Delta G_A^{elas}) + \gamma_{MX-A}S_{MX-A}.$$

Here, $G_{MX}^{\circ}$ and $G_A^{\circ}$ are the standard changes in the Gibbs energies of the formation of individual components MX and A; $\gamma_{MX}S_{MX}$ and $\gamma_A S_A$ are their excess surface energy determined by the specific surface energy ($\gamma$) multiplied by the free surface area; $\Delta G_{MX}^{elas}$ and $\Delta G_A^{elas}$ are the elastic strain contributions; $\gamma_{MX-A}S_{MX-A}$ is the energy of the interface, where $\gamma_{MX-A}$ is the specific surface energy at the interface; $S_{MX-A}$ is the area of the contact between components MX and A; the contribution of the elastic energy is taken into account by terms $\Delta G_{MX}^{elas}$ and $\Delta G_A^{elas}$. The expression for the Gibbs energy of the component MX can be obtained from Eqn (17), if we assume that the interface energy is evenly distributed between the components

$$G_{MX} = G_{MX}^{\circ} + \gamma_{MX}S_{MX} + \frac{\gamma_{MX-A}S_{MX-A}}{2} + \Delta G_{MX}^{elas}. \quad (18)$$

The contribution of elastic strains ($\Delta G_{MX}^{elas}$) to the total energy of the MX phase is largely determined by the elastic energy of the misfit in lattice parameters at the interface and the energy of dislocations that arise in the interface regions. The calculations of $G^{elas}$ even for thin films with simple morphologies are very tedious; hence, it is difficult to assess this contribution in composites. Nonetheless, in all the cases irrespective of the nature of elastic strains (dilatational or compression strains), the quantity $\Delta G_{MX}^{elas}$ is positive and should increase with an increase in $S_{MX-A}$. Hence, the last two terms in expression (18), which determine the energy of the MX phase depend on the area of the interphase contact in the composite.

Sintering of a mixture of a low-melting component MX (with the higher self-diffusion coefficients) with the nanoparticles of a high-melting component A can be accompanied by both a decrease and an increase in the interface area. In the former case, the sintering is reduced to simple recrystallisation of phases. The latter case is more interesting for solid-state chemistry. The process of the formation of an interphase contact (Fig. 7) is thermodynamically favourable if $dG/dS_{MX-A} < 0$. In this case, the sintering is accompanied by an increase in the interface area $S_{MX-A}$. If we ignore the dependences of the specific surface energies and the elastic energy on the surface area (or the particle size) [$\gamma_{MX}$, $\gamma_A$,

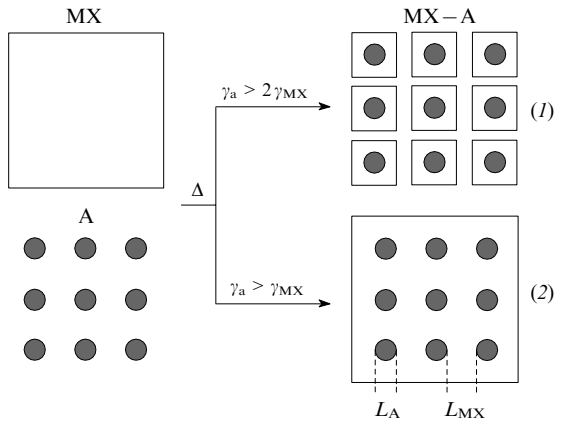



**Figure 7.** Illustration of self-dispersion of an ionic salt MX at its contact with a nanocrystalline oxide A (see the text).

$\gamma_{MX-A}$, $G_{MX}^{elas}$, $G_A^{elas} \neq f(S_{MX-A})$] and express $\gamma_{MX-A}$ through the free energy of adhesion ($\gamma_a$)

$$\gamma_a = \gamma_{MX} + \gamma_A - \gamma_{MX-A},$$

we can find the change in the Gibbs energy of a composite with the increase in the interface area by $dS_{MX-A}$

$$\frac{dG}{dS_{MX-A}} = \gamma_{MX}\frac{dS_{MX}}{dS_{MX-A}} + \gamma_A\frac{dS_A}{dS_{MX-A}} + \gamma_{MX} + \gamma_A - \gamma_a. \quad (19)$$

Pines [85] and Geguzin [86] considered in detail the mechanism of sintering, *i.e.*, the formation and the growth of the interface. The mechanism and kinetics of sintering differ for two cases determined by the conditions $\gamma_a < 2\gamma_{MX}$ and $\gamma_a > 2\gamma_{MX}$. In the former case, a neck is formed between two grains the shape and size of which are determined by the shape and size of particles and the absolute magnitudes of $\gamma_{MX}$, $\gamma_A$ and $\gamma_a$.

The expression

$$\gamma_a > 2\gamma_{MX} \quad (20)$$

is known as the Gibbs–Smith condition for complete spreading. It can be derived from Eqn (19), provided that $dG/dS_{MX-A} < 0$, $dS_A/dS_{MX-A} = -1$, $dS_{MX}/dS_{MX-A} \approx 1$, *i.e.*, if the decrease in the free energy of a component A (substrate) is accompanied by the formation of the equivalent free surface of a component MX (film). The same condition is prerequisite for the stable layer-by-layer growth of films according to the Frank–van der Merve mechanism. Figure 7 (*1*) shows the corresponding changes in the morphology. However, upon sintering of mixtures with an arbitrary microstructure, the newly formed free surfaces of the component MX can overlap if the distances between the surfaces of phase A are sufficiently small [Fig. 7 (*2*)]. At the complete overlap of free surfaces, the derivative $dS_{MX}/dS_{MX-A}$ approaches zero, and the following expression can be derived from Eqn (19):

$$\gamma_a > \gamma_{MX}, \quad (21)$$

which represents a condition of the feasibility in principle of spreading of the component MX over the surfaces of the phase A in a composite. A comparison of condition (21) with the condition (20) for the complete spreading (or epitaxy) in films shows that the interfacial interaction in composites should proceed more actively and at lower energies of adhesion in contrast to ordinary film structures. The surface roughness is known to improve wettability. The roughness coefficient is equal to the ratio of the true contact area to its apparent area and can take values in the range from zero to unity. Equation (21) corresponds to the limiting roughness coefficient of the phase A equal to unity.

If conditions (20) or (21) are met, the interface area in the system spontaneously increases or the sufficiently well developed surface of nanocrystals A is 'wetted' with the substance MX. A comparison of values $\gamma \approx 100-300$ erg cm$^{-2}$ for alkali metal halides [87] with the specific surface energies of oxides $Al_2O_3$, FeO, MgO and $SiO_2$ ($\gamma \approx 600-1200$ erg cm$^{-2}$) (Refs 88 and 89) suggests that the wetting condition (20) should be fulfilled for composites that consist of ionic halides and high-melting oxides including alumina.

If substance A is in the nanocrystalline state, the effective size of particles of the phase MX should decrease to very small values, *i.e.*, an unusual effect, the self-dispersion of component MX to form a two-phase nanocomposite is observed.[24] Indeed, the self-dispersion effect was observed during the solid-phase sintering of composites $AgCl-Al_2O_3$,[60] $AgI-Al_2O_3$ (Refs 61, 71 and 90–92) and $Li_2SO_4-Al_2O_3$.[82, 83, 93, 94] A similar effect was observed in heterogeneous systems based on alkali metal nitrates [$LiNO_3-Al_2O_3$, $NaNO_3-Al_2O_3$,[95] $RbNO_3-Al_2O_3$,[67, 96, 97] $CsNO_3-Al_2O_3$ (Ref. 96)] and halides [$NaCl-Al_2O_3$, $KCl-Al_2O_3$ and $RbCl-Al_2O_3$ (Ref. 24)], which points to the good adhesion of ionic salts to the alumina surface. Self-dispersion serves as the indicator of strong interfacial interaction in the system and occurs at long-term sintering until the whole surface of the component A is covered with substance MX. In this limiting case, the quantity $S_{MX-A}$ approaches $S_A$, and the system spontaneously reaches firm metastable equilibrium where

$$G = (G_{MX}^{\circ} + G_A^{\circ}) + \gamma_{MX-A}S_A + \left(\Delta G_{MX}^{elas} + \Delta G_A^{elas}\right),$$

$$G_{MX} = G_{MX}^{\circ} + \frac{\gamma_{MX-A}S_A}{2} + \Delta G_{MX}^{elas}. \quad (22)$$

According to the latter expression, the properties of an ionic salt are determined not only by the standard thermodynamic parameters of the substance, but also by the contribution of the energy of interfacial interaction, which increases in proportion to the surface area of the oxide A (or in the inverse proportion to the size of its particles). If the components taken in a volume ratio of 1 : 1 are uniformly mixed so that the total surface of a component A is completely wetted with a component MX, the effective size of MX grains is approximately equal to $L_A/2$. In composites with oxide nanoparticles ($L_A/2 \approx 10$ nm), the size of MX particles becomes sufficiently small for the manifestation of pronounced size effects.

## VII. Size effects in composites

Size effects in heterogeneous systems [84] are determined by many factors, namely, the chemical nature of components in the heterogeneous mixture, the morphology of the system and the interfacial interaction between the components. Since it is difficult to take into account these factors, no adequate theoretical description of the size effect in composites has been developed so far. As in the case of pure substances, the most pronounced changes in the properties are observed in nanocomposites, *i.e.*, heterogeneous systems with the average size of particles of both phases below100 nm. In recent years, the interest in the unusual effects observed in nanosize systems has arisen.[17–22, 24, 84, 85, 88, 98–128] This is not surprising, since the processes that involve nanosystems form the basis for future solid-state nanotechnologies.

Size effects can conditionally be divided into two types.

1. Weak effects, where the physicochemical properties of a substance change insignificantly with an increase in the specific surface area (or a decrease in the particle size) and all the changes observed can be explained by the additive effect of the

surface on the basic properties of a crystal. According to the classification proposed by Shcherbakov,[129,130] these effects may be assigned to capillary effect of the first kind. As a rule, these effects are observed in crystals with the size above 10 nm.

2. Strong phase size effects or, according to the Shcherbakov classification, capillary effects of the second kind responsible for the qualitative changes in the substance properties, which are impossible to explain in terms of ordinary surface phenomena. As a rule, these effects are observed in very small particles the size of which does not exceed 10 nm. It is these systems that should be considered as truly nanosize systems. The concept of Shcherbakov was qualitatively confirmed by the subsequent experimental and theoretical studies [84,100–104,116,117,124,126].

As a result of spreading or self-dispersion, the Gibbs energy of an ionic salt increases to a value described by expression (22). The excess energy is determined by two main factors, namely, the interface energy, which depends on the nature and the energy of interactions between the surface atoms of phases in contact, and the elastic strains that arise in the bulk of contacting phases.

The mechanism of interactions in composites MX–A is determined by the contribution of non-dispersion interactions, namely, ion–ion, donor–acceptor, dipole–dipole, *etc*. The correct estimation of the interface energy requires consideration of the structure of the contact plane and the real potentials of ion–ion interactions in the contact region, which is an extremely complicated and still unsolved problem. It was shown [24] that lithium salts in systems with alumina exhibit a stronger trend for the formation of nanocomposites as compared with rubidium and caesium salts, while iodides more readily form nanocomposites as compared with chlorides and fluorides. This suggests that the polarising power of the cation and the polarisability of the anion in the ionic component play an important role in the surface interaction mechanism.

Studies of thin films have demonstrated that the structure of a solid in the near-interface region depends substantially on the features of the crystallography and energy of planes in contact. As a rule, in very thin films, the epitaxal contact between phases is energetically favourable and the film structure is determined by the effect of the support and can differ from the structure of the same substance in the individual state. With the increase in the film thickness, elastic strains are accumulated in its bulk, which results in the film restructuring upon reaching a certain critical thickness $h_{cr}$. For a minor misfit in the structural parameters, the film acquires a structure corresponding to the pure component and a network of misfit dislocations is formed on the interface. For a 1%–0.1% misfit in the lattice parameters, the thickness of the epitaxial layer was calculated to be $h_{cr} \approx 5–25$ nm.[131–133] If the structural parameters of the substrate and the film differ substantially, $h_{cr}$ becomes very small, and the relaxation of the elastic energy of the growing epitaxial layer necessitates the formation of a very large number of dislocations, which becomes energetically unfavourable. In this case, the relaxation of elastic strain energy can proceed through different channels, namely, the film can be divided into separate blocks the size of which increases with the increase in the film thickness or an amorphous surface phase is formed.[100,133]

In the above-mentioned cases, the formation of thin epitaxial, nanocrystalline or amorphous films may be considered as the manifestation of the phase size effect in heterogeneous systems, *viz*., with the increase in the characteristic size (film thickness), new surface phases are formed.

In the composites MX–A the distance between the grains of the oxide component A plays the role of the MX layer thickness. If the size of particles A far exceeds $h_{cr}$, the properties of the ionic component are similar to those of thick MX films. If the oxide grains are sufficiently small and comparable with $h_{cr}$, then at sufficiently high oxide concentrations, the MX phase is localised in nanopores between oxide particles, *i.e*., under the conditions similar to those of the existence of a thin MX layer on the surface of A. In a real composite, two states always coexist (a 'normal' state of coarse MX grains and an 'interfacial' state with anomalous properties) in a quantitative ratio determined by the composition and morphology of the composite.

The thermodynamic properties of substances deposited on a solid support to form adsorbed layers or thin films differ from those in the bulk.[85,98–100,131] The characteristic grain size at which noticeable deviations in the thermodynamic properties are observed is $\sim 10$ nm.[84,100–102,105,107–111,113,116,117,124] The temperature of a phase transition ($T_t$) that occurs in the bulk of an ionic salt MX can be estimated [24,100,115] using the following approximate relationship:

$$\frac{T_t}{T_t^\circ} = 1 - \left[(\gamma^\beta_{MX} S^\beta_{MX} - \gamma^\alpha_{MX} S^\alpha_{MX}) + \right.$$

$$\left. + \frac{1}{2}(\gamma^\beta_{MX-A} S^\beta_{MX-A} - \gamma^\alpha_{MX-A} S^\alpha_{MX-A}) + \Delta G^{elas}\right] \frac{1}{H_t},$$

where $T_t^\circ$ is the standard temperature of the transition, superscripts α and β correspond to high-temperature and low-temperature phases, respectively, $\Delta G^{elas}$ is the difference between the excess elastic energies of phases β and α, $H_t$ is the enthalpy of the phase transition. The interface energies $\gamma_{MX}$ and $\gamma_{MX-A}$ decrease with the increase in the temperature; this is why if the phase transition is accompanied by only small changes in the bulk and $\Delta G^{elas}$ ($S^\alpha_{MX} \approx S^\beta_{MX} \sim L^{-1}_{MX}$; $S^\alpha_{MX-A} \approx S^\beta_{MX-A} \sim L_A^{-1}$; $\Delta G^{elas} \approx 0$), the temperature of transformation to the high-temperature α-phase will decrease, which indeed was usually observed for thin films where the layer thickness plays the role of the particle size. The literature offers two types of phase diagrams plotted in coordinates $T_t(T,L^{-1})$ for supported films of different metals;[85,98–100] the phase transition temperatures can decrease by hundreds of degrees as $L$ decreases to 10 nm. In the general case, the phase transition temperatures in a composite can either decrease or increase depending on the concrete form of functions $G^\circ = f(T)$; $\sigma = f(T)$; $\Delta G^{elas} = f(T)$ in different phases of a given composite.

The above-described self-dispersion effect caused by the surface interaction of ionic salts with nanodispersed oxides (the particle size not exceeding 10 nm) allowed a wide range of nanocomposites of the MX–A type to be synthesised and studied.[24,84,134–148] Ionic salts in the nanoheterogeneous systems mentioned exhibited several specific features.

1. Crystal structure and morphology. In sintered composites $AgI–Al_2O_3$,[61,71,90–92] either various polytypes or an amorphous phase were formed depending of the oxide particle size and the conditions of the composite synthesis. Nanocomposites synthesised at 600 °C comprised globular AgI particles measuring 2–5 nm and uniformly distributed over the composite volume (Fig. 8). According to the results of structural studies of composites $LiX–Al_2O_3$ ($X^- = F^-$, $Cl^-$, $Br^-$, $I^-$, $1/3\,PO_4^{3-}$, $1/2\,SO_4^{2-}$) synthesised by decomposition of a precursor, the size of particles in both phases of the composite did not exceed 10 nm, *i.e*., solid-phase nanocomposites were formed.[53] The most thoroughly studied nanocomposites $Li_2SO_4–Al_2O_3$ exhibited the highest conductivity among these nanocomposites.[53,82,83,93,94] On the interfaces of these composites, regardless of the method of their synthesis [by decomposition of the precursor $Li_2SO_4 \cdot 2n\,Al(OH)_3 \cdot m\,H_2O$ or by simple mixing of components followed by sintering], an intermediate aluminate layer with a thickness of about 1–2 monolayers was formed to provide a good epitaxial contact

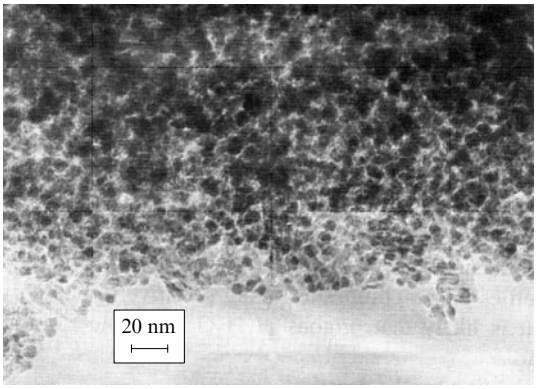



**Figure 8.** Morphology of the nanocomposite $0.2\,AgI-0.8\,Al_2O_3$ synthesised at 600 °C.

between $Li_2SO_4$ and $Al_2O_3$. The average particle size varied in the range of 3–10 nm (Fig. 9). In composites $CsCl-Al_2O_3$, according to the X-ray diffraction data, a high-temperature face-centred CsCl phase with the particle size in the range of 20–80 nm was stabilised.[144] In nanocomposites based on alkali metal nitrates, amorphous phases of ionic salts were formed.[67, 95–97]

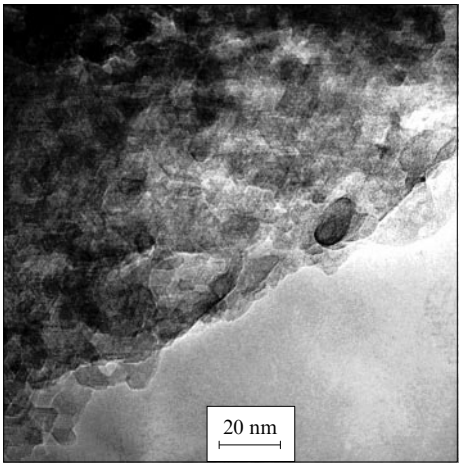



**Figure 9.** Microstructure of the composite $Li_2SO_4-Al_2O_3$.

2. Thermodynamic properties. Rubidium nitrate attracts attention because in the temperature range of 25–330 °C it undergoes three polymorphous transitions (at 164, 219 and 286 °C) before melting at 315 °C. The results of differential scanning calorimetry (DSC) studies of composites $RbNO_3-Al_2O_3$ showed [67] that sintering did not virtually affect the temperatures of all phase transitions of rubidium nitrate including the melting temperature, while the corresponding enthalpies dramatically decreased (Fig. 10*a*). At a relatively low mole fraction of the oxide ($x \geqslant 0.7$), the curves demonstrated no heat effects that would point to the presence of crystalline rubidium nitrate in the composite. In line with the decrease in the enthalpy of crystalline $RbNO_3$, the DSC curves acquire a new strongly broadened peak at 250 °C. The mentioned effects were not observed in composites containing coarse-grained alumina (with the grain size of several micrometres); hence, the effects were intrinsic in the oxide surface (Fig. 10*b*). In composites $RbNO_3-Al_2O_3$, an amorphous phase was formed and the heat effect at 250 °C was caused by the phase transition, namely, its vitrification. The formation of an amorphous phase in nanocomposites was also confirmed by

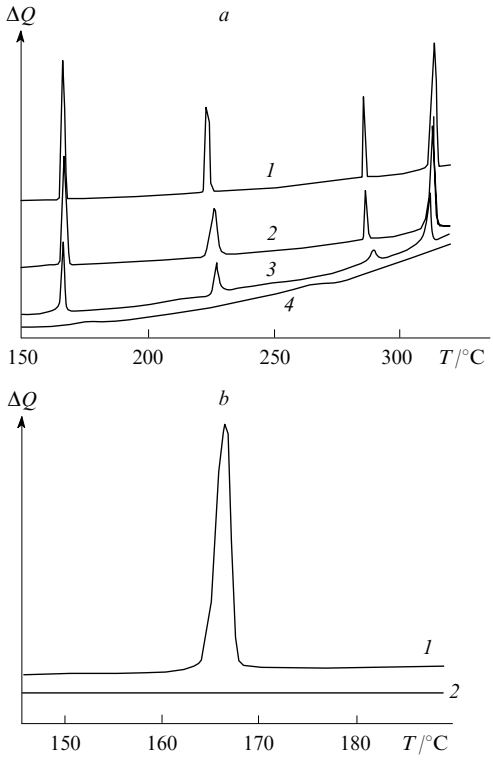



**Figure 10.** (*a*) DSC curves of composites $(1-x)\,RbNO_3-x\,Al_2O_3$ [$x$ = 0.1 (*1*), 0.3 (*2*), 0.5 (*3*), 0.7 (*4*)] containing nanocrystalline alumina ($S_{sp}$ = 270 $m^2\,g^{-1}$), which were heated at 350 °C and (*b*) segments of DSC curves in the region of phase transition $RbNO_3$-IV ⇄ $RbNO_3$-III for the composites $0.3\,RbNO_3-0.7\,Al_2O_3$ containing (*1*) coarse-grain and (*2*) nanocrystalline alumina.

the disappearance of the heat effect associated with salt melting. The amorphisation of an ionic salt also occurred in composites $RbNO_3-SiO_2$,[145] $CsHSO_4-SiO_2$ (Refs 146 and 147) and $LiClO_4-Al_2O_3$ (Ref. 148). In composites $CsCl-Al_2O_3$, with the increase in the oxide concentration, the enthalpy of the transition to the high-temperature phase gradually decreased, which was accompanied by the broadening of the hysteresis loop of the phase transition temperature.[144]

Expression (11) allows one to assess the ratio $\lambda/L_A$ and, for a given particle size ($L_A$), the thickness of the surface phase ($\lambda$), based on the concentration dependence of the enthalpy of phase transitions in composites. The $\lambda$ estimates were 3 and 4 nm in composites $AgI-Al_2O_3$ (Ref. 92) and $RbNO_3-Al_2O_3$ (Ref. 97), respectively. For a sufficiently high concentration of the oxide ($x > 0.6-0.7$, which corresponds to the volume ratio $f > 0.5-0.6$), the effective size of MX particles was comparable with $\lambda$ and virtually the whole volume of the ionic salt was in the amorphous state (Fig. 11).

Self-dispersion of rubidium nitrate in contact with nanocrystalline alumina (the specific surface of 200 $m^2\,g^{-1}$) was studied [97, 149] *in situ* by the DSC method; the results are shown in Fig. 12. For non-mixed starting components, the surface interaction began at the rubidium nitrate melting temperature, as indicated by the appearance of the exothermic effect. In the melting, the liquid-phase spreading occurred being accompanied by liberation of the heat of wetting. The DSC curves obtained in the repeated heating of the same specimen corresponded to a mixture of the residual crystalline and amorphous phases. When the starting components were mixed more thoroughly, the surface dispersion and self-dispersion proceeded at noticeable rates even at temperatures substantially

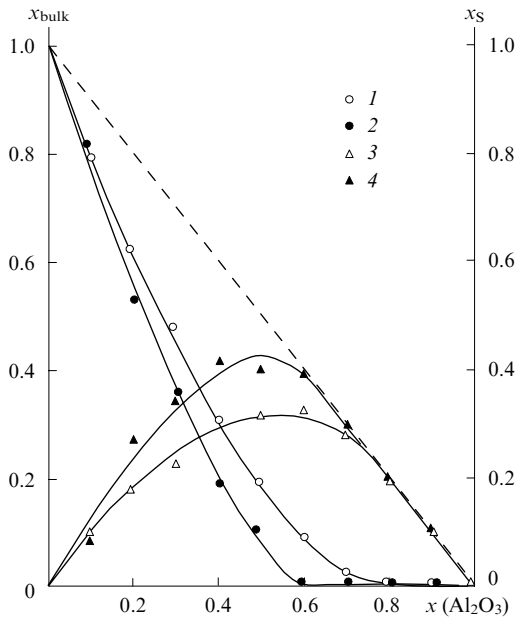



**Figure 11.** Mole fractions of (*1*, *2*) bulk ($x_{bulk}$) and (*3*, *4*) surface ($x_S$) phases in composites (*1*, *3*) $(1-x)\,AgI-x\,Al_2O_3$ (Ref. 92) and (*2*, *4*) $(1-x)\,RbNO_3-x\,Al_2O_3$ (Ref. 67) as a function of the additive content. Experimental values were calculated from the enthalpy of phase transitions. Theoretical curves were obtained based on Eqn (11). The dashed curve corresponds to the case of $\lambda/L_A = 0$ where the composite altogether lacks the surface phase.

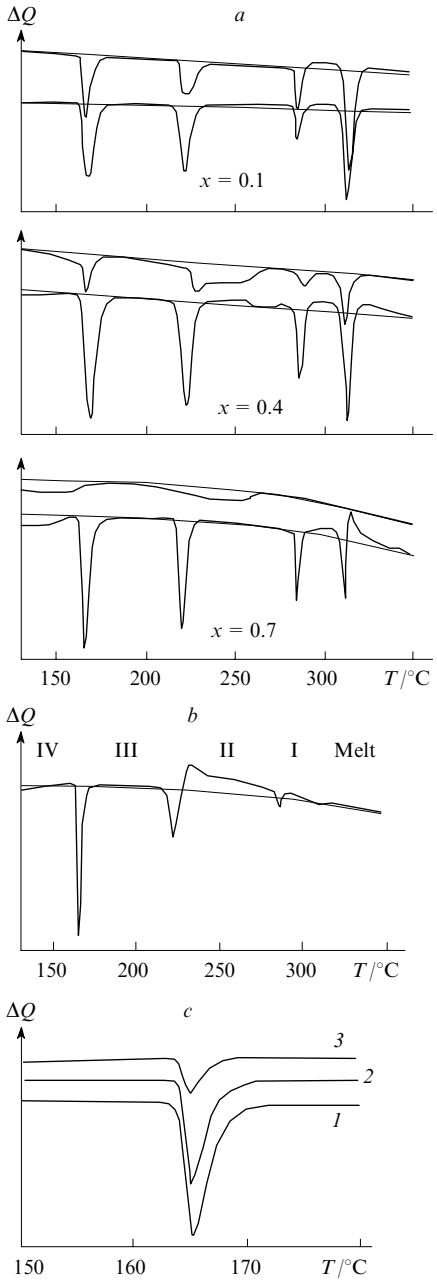



**Figure 12.** (*a*) DSC curves of original $RbNO_3-Al_2O_3$ mixtures (lower curves) and the same mixtures in repeated heating (upper curves) for different component ratios; (*b*) a DSC curve of a thoroughly ground mixture $0.6\,RbNO_3-0.4\,Al_2O_3$ obtained in the first heating and (*c*) a comparison of a segment of this curve (*1*) with the corresponding segments of DSC curves measured after 1-h exposure of this mixture to temperatures (*2*) 200 and (*3*) and 250 °C.

below $T_{mp}$, *i.e.*, where rubidium nitrate was in the crystalline state. Due to the solid-phase spreading, the amorphous phase was formed, *i.e.*, the crystalline phase spontaneously passed to the amorphous state. The solid-phase spreading to form the amorphous phase was also observed upon sintering of composites $AgI-Al_2O_3$.[92]

The possible reason for the spontaneous amorphisation of an ionic salt MX in the composites MX–A due to the liquid-phase or solid-phase spreading could be the relaxation of elastic strains that arise in the MX volume formed as a result of the salt spreading over the surface and in the pores of the oxide matrix. If the lattices of the contacting phases do not match one another, the contribution of the elastic energy becomes substantial. Moreover, in contrast to thin films, the MX particles in nanopores are adhesively bound with the randomly oriented oxide surfaces surrounding a pore, which should lead to rather active formation of microdomains of particles and provide the excess surface energy. Apparently, the structural relaxation can occur by spontaneous amorphisation of an ionic salt. This process may be illustrated by a phase diagram shown in Fig. 13.[97,139,140] The amorphisation is possible if with the decrease in the effective particle size, the free energy of the crystalline MX phase becomes higher than the energy of the amorphous phase. A concept of the spontaneous transition from the crystalline to the amorphous state was discussed earlier in the literature in context of the reasons for the mechanical alloying of ionic salts.[150–158] The data on the amorphisation of alkali metal halides[159,160] and certain other inorganic crystalline hydrates[161–167] in nanopores are available. Amorphous hydrates incorporated into nanoporous matrices turned out to exhibit unusual thermodynamic properties, which are responsible for the changes in the parameters of chemical processes of hydration and dehydration.

3. Ionic conductivity and dielectric properties. In the low-temperature range, all the nanocomposites $(1-x)\,AgI-x\,Al_2O_3$ studied exhibited enhanced ionic conductivity.[61,71,90–92] A comprehensive analysis of the temperature dependence of conductivity and the results of calorimetric studies of composites revealed the presence of two phase transitions. The temperature dependences of conductivity had a non-trivial shape, namely, with the increase in $x$, the phase-transition hysteresis gradually widened and the conductivities of the high-temperature (superionic) and low-temperature phases gradually became equal, *i.e.*, the phase transition of a salt to the superionic state gradually disappeared[61,71,91] (Fig. 14*a*). The conductivity maximum ($\sim 10^{-3}$ S cm$^{-1}$ at 25 °C) was situated not at $x = 0.20-0.30$ as was observed earlier but at a higher mole fraction of the oxide, $x = 0.5-0.6$

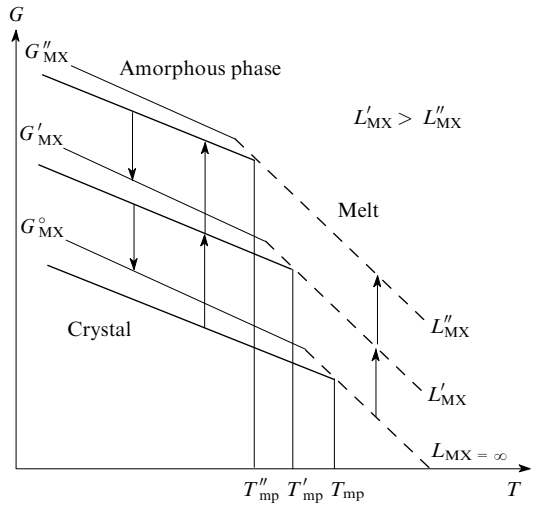



**Figure 13.** State diagram of an ionic salt in a composite; the changes in the energy of the system in the amorphisation of ionic compounds are indicated.

(Fig. 14*b*). The activation energy of conduction in both superionic and low-temperature phases increased monotonically with the increase in $x$. The concentration dependence of the dielectric permittivity $\varepsilon(x)$ had two maxima, namely, the first weak maximum at $x = 0.2$ and the second more pronounced maximum at $x = 0.9$ (see Fig. 14*b*).[92] These results are consistent with the percolation model [11] according to which the permittivity maxima corresponding to two percolation thresholds should be observed at the oxide volume fractions $p_1 = 0.1$ and $p_2 = 0.9$ (*i.e.*, at $x = 0.12$ and 0.94).

The temperature dependence of conductivity of the nanocomposite $Li_2SO_4-Al_2O_3$ lacked the conductivity jump at 575 °C associated with the transition of lithium sulfate to the superionic state (Fig. 15).[82, 83, 93, 94] The $\sigma(T)$ dependence had a shape typical of solid electrolytes with the fluorite structure in the vicinity of the 'diffuse' phase transition.

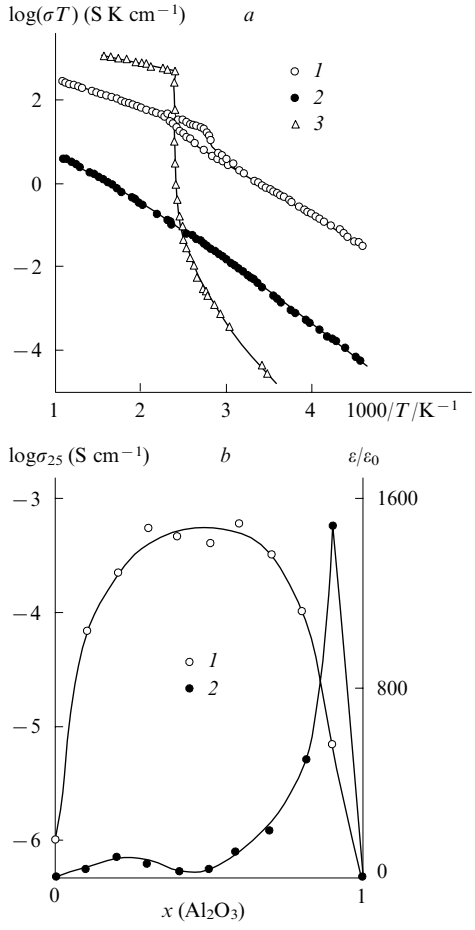



**Figure 14.** (*a*) Temperature dependences of conductivity ($\sigma T$) of composites $(1-x)AgI-x\,Al_2O_3$ [$x = 0.60$ (*1*), 0.80 (*2*), 0 (*3*)] and (*b*) isotherms of their (*1*) conductivity and (*2*) permittivity at room temperature.[92]

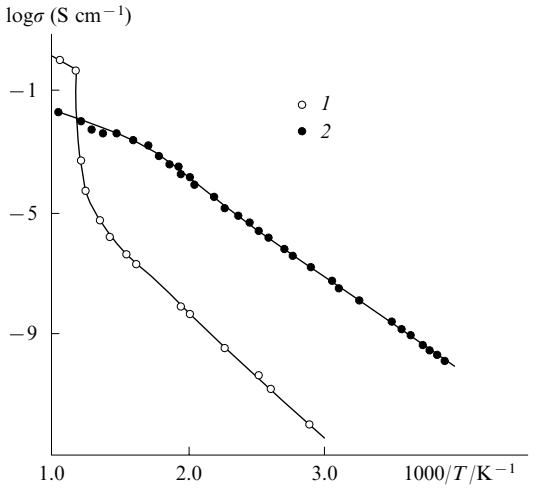



**Figure 15.** Temperature dependences of conductivity of (*1*) pure lithium sulfate and (*2*) a nanocomposite $Li_2SO_4-Al_2O_3$.[82]

Studies of the conductivity of composites based on alkali metal nitrates $MNO_3-Al_2O_3$ (M = Li, Na, K, Rb, Cs) have shown [95, 96] that doping of nitrates with alumina with a specific surface area of 270 m$^2$ g$^{-1}$ is accompanied by a sharp increase in the conductivity (Fig. 16). The dependences of the conductivity on the dopant concentration had a maximum at $x = 0.5-0.7$, and the relative increase in the conductivity

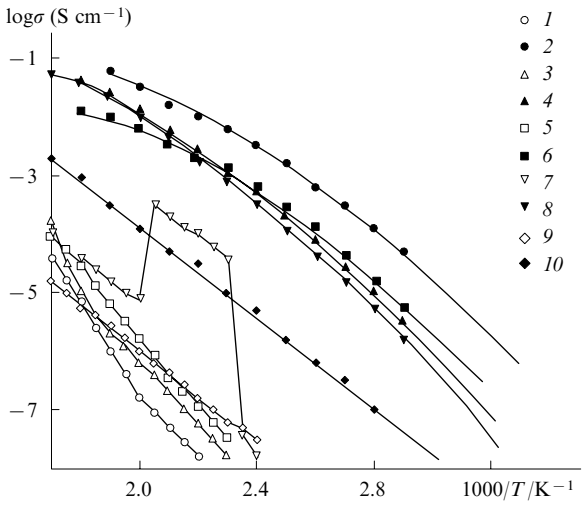



**Figure 16.** Arrhenius plots of conductivity for (*1*, *3*, *5*, *7*, *9*) pure alkali metal nitrates and (*2*, *4*, *6*, *8*, *10*) a 1 : 1 composite $MNO_3-Al_2O_3$.[95, 96] M = Li (*1*, *2*), Na (*3*, *4*), K (*5*, *6*), Rb (*7*, *8*), Cs (*9*, *10*).

$(\sigma/\sigma_o)$ at 343 K depended on the cation type and varied in the range from $10^2$ (in composites $CsNO_3-Al_2O_3$) to $10^8$ (in composites $LiNO_3-Al_2O_3$). For $x > 0.5-0.6$, the Arrhenius plots $\sigma(T)$ of all composites studied were not linear and lacked conductivity jumps at phase transition temperatures. The physicochemical properties of composites based on rubidium nitrate were studied in more detail. The decomposition voltage $U_d = 4$ V assessed from voltammetric curves was close to the corresponding values in fused alkali metal nitrates and halides which allows one to assume that rubidium cations are the main current carriers in the composites $RbNO_3-Al_2O_3$.

In the composites $CsCl-Al_2O_3$, with the increase in the oxide concentration, the conductivity jump associated with the transition to the high-temperature phase gradually disappeared, which was associated with the stabilisation of the latter phase (Fig. 17).[144]

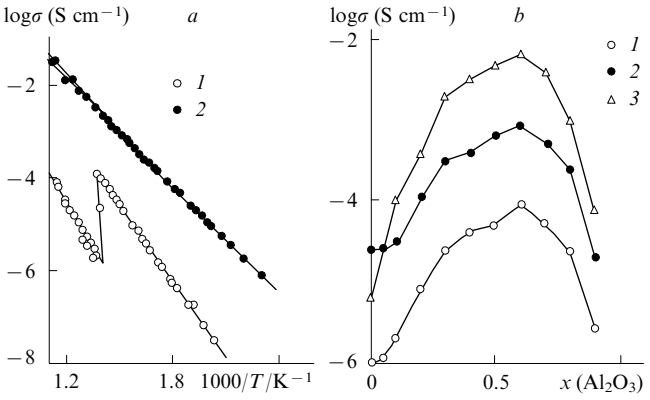



**Figure 17.** Dependences of conductivity of composites $(1-x)\,CsCl-x\,Al_2O_3$ (*a*) on the temperature and (*b*) and the oxide concentration.
(*a*) $x = 0$ (*1*), 0.60 (*2*); (*b*) $T = 573$ (*1*), 673 (*2*) and 773 K (*3*).

Thus, in all systems under study, the nature of conduction was observed to change at sufficiently high concentrations of the fine-grain additive. These changes can be associated with either the appearance of new highly conductive amorphous phases atypical of pure ionic compounds (composites based on nitrates, $AgI-Al_2O_3$) or with the stabilisation of high-temperature phases (the phase-transition hysteresis in $Li_2SO_4-Al_2O_3$ and $AgI-Al_2O_3$, the formation of a face-centred cubic phase in $CsCl-Al_2O_3$) in composites. Moreover, the properties of high-temperature phases stabilised in nanocomposites differed from those of the same phases in pure salts, namely, the former had higher activation energies and modified lattice parameters. A clear trend for the levelling of the characteristics of high-temperature and low-temperature phases was observed, the phase transition region widened and the transition itself became diffuse approaching the second-order phase transitions. Nanocomposites differ basically from polycrystals and microcomposites in their properties; this is explained by the increasing effect of surface interactions on the bulk properties of ionic salts. Under certain conditions, this leads to the appearance of phase size effects or capillary effects of the second kind. Figure 18 illustrates the changes in the ionic salt structure in the vicinity of the MX – A interface, which were observed as the surface interaction increased, *i.e.*, on going from micro- to nanocomposites.

Computer simulation methods can be used for the elucidation of the nanocomposite structure and the conduction mechanism. Nanocomposites $LiI-Al_2O_3$ were studied [168] by the molecular dynamics techniques. It was shown that the phase contact was epitaxial, the electrical double layer was

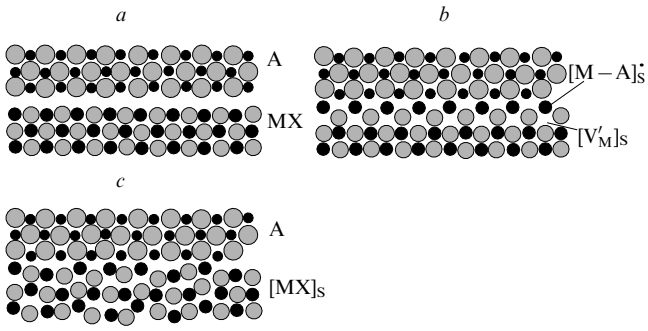



**Figure 18.** Changes in the ionic salt structure in the vicinity of the MX – A interface with the increase in the effect of surface on the bulk properties of MX, *i.e*, on going from micro- to nanocomposites.
(*a*) Original surfaces; (*b*) weak interfacial interaction, insignificant structural changes, the capillary effect of the first kind; (*c*) interfacial interaction generates dramatic changes in the ionic salt structure (*e.g.*, amorphisation), phase size effect, the capillary effect of the second kind.

formed at the interface and the activation energy of diffusion of lithium cations was close to the experimental value.

The molecular dynamics methods were also applied [169] for the simulation of the $CsCl-\alpha$-$Al_2O_3$ interface. The calculation model represented a two-layer heterostructure that comprised 22 080 ions (3840 ions of $Cs^+$ and $Cl^-$ each and the balance number of $Al^{3+}$ and $O^{2-}$ ions). The calculations were performed for cyclic boundary conditions and involved the use of the Born – Mayer potential. The parameters of the potential were taken from the literature and refined in the preliminary simulation of individual starting components $Al_2O_3$ and CsCl. The heterostructure was obtained as a result of spontaneous crystallisation of a model CsCl melt, which was followed by the long-term isothermal exposure at $T = 0.8T_{mp}$ up to the establishment of the steady state (Fig. 19). Caesium chloride crystallised to form a high-temperature phase structure of the NaCl type and did not pass to the low-temperature state as the temperature decreased. The $CsCl-\alpha$-$Al_2O_3$ interface was realised along the (110) CsCl || $(10\bar{1}0)$ $Al_2O_3$ planes which were off-oriented by a small angle of $\sim 10-13^\circ$ and contained boundary dislocations at a distance of $\sim 5$ nm from one another. The boundary dislocations corresponded to the sites of the surface exposure of low-angle boundaries localised in the caesium chloride bulk. Although the bulk of caesium chloride as a whole represented a monolythic crystal, the low-angle boundaries divided it into two microdomains disoriented by $3-3.5^\circ$.

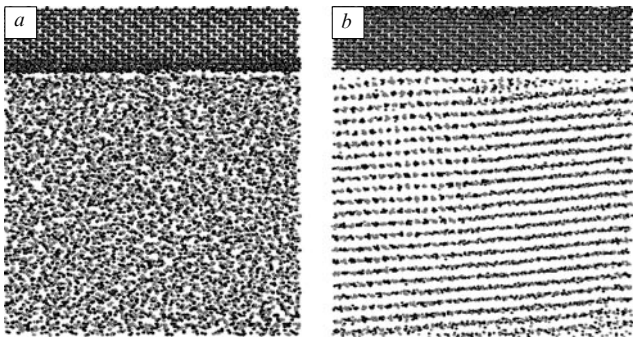



**Figure 19.** Heterostructure $CsCl-Al_2O_3$ calculated by the molecular dynamics method.[169]
(*a*) For temperatures above the melting point of caesium chloride; (*b*) immediately after its hardening and isothermal exposure at $T = 0.8T_{mp}$.

In contrast to the system $LiI-Al_2O_3$, no double layer was formed on the interface. Nonetheless, the ions located in the vicinity of the interface and on low-angle boundaries exhibited enhanced mobility. The self-diffusion coefficients of caesium and chloride ions were approximately the same, *i.e.*, equal to $\sim 10^{-6}$ cm$^2$ s$^{-1}$ at 700 K, which is smaller than the corresponding values in molten CsCl by merely an order of magnitude. Apparently, the main difference of the system $CsCl-Al_2O_3$ from the system $LiI-Al_2O_3$ is the weak interface interaction. In this case, it is the energy of elastic strains the relaxation of which favours the appearance of intergrain dislocations and small-angle boundaries that makes the main contribution to the changes in the ionic salt properties. Hence, the real composite structure and the mechanism of ionic conduction in nanosized systems depend not only on the energy of interactions, but also on the energy of elastic strains that arise in the interface zone.

The spectrum of phenomena observed in nanocomposites is very wide. Particularly, nanocomposites with protonic conductivity, which are based on acid salts, were shown to exhibit interesting properties.[146,170–176] In our studies, we have shown that the physicochemical characteristics of ionic salts depend on the pore size in the silica gel used as the dispersed additive, *viz.*, there is an optimum pore size ($\sim 2$ nm) corresponding to the maximum changes in the thermodynamic, structural and transport properties of $CsHSO_4$.[170] In our studies, we deliberately ignored the systems with chemical interactions between the components. The chemical reactions make possible the formation of three or four-layer components that include the starting reagents and interfacial phases.[177] Recent years were marked by the discovery of metacomposites, *i.e.*, heterogeneous systems the interfacial interaction in which brings substantial changes into the physicochemical properties of both components.[149,178] Moreover, such a heterosystem as a whole exhibits the properties typical of none of its individual components. Such materials form a new interesting class of metamaterials. The transport properties of metamaterials synthesised by the layer-by-layer deposition of nanolayers $CaF_2/BaF_2$ were studied.[179,180] Nanostructurised solid solutions[181–183] the lattices of which contain separate nanodomains coherently attached to one another and divided by interdomain boundaries are of special interest for solid-state ionics. Highly doped superionic fluorides that comprise extended clusters in their structure are another example of nanoheterogeneous systems.[184] It is not improbable that nanostructuring is the general property of highly doped solid solutions.

Nanoheterogeneous solid-phase systems are of great interest for practice. Like all composite solid materials, they are characterised by the enhanced mechanical strength and thermal stability and can be used in chemical power sources, gas sensors and other electrochemical devices. The high ionic conductivity is among the most important characteristics of nanocomposite solid electrolytes. Nanocomposites based on conventional ionic salts far surpass the corresponding polycrystalline materials and microcomposites in the conductivity. Another valuable characteristics of these materials is that the phase transitions in them are absent or levelled off, which prevents the loss of their mechanical strength at thermal cycling. In model medium-temperature fuel cells with a nanocomposite solid electrolyte $CsHSO_4-SiO_2$, sufficiently high current densities were reached.[185,186] The performance of a fuel cell with a composite electrolyte compares well with the performance of a cell that employs pure salt as the electrolyte.[187] Nanocomposites $LiClO_4-Al_2O_3$ exhibit high lithium conductivity at 150–200 °C.[148] Studies of medium-temperature lithium cells with solid electrolytes and oxide electrodes were initiated.[188]. Further miniaturisation of these devices, the decrease in the electrolyte thickness and the optimisation of characteristics of electrode materials may provide high power of batteries.

## VIII. Conclusion

Summarising the results of studies of composite ionic conductors, it may be concluded that the properties of composite solid electrolytes are determined by both the intrinsic disordering of an ionic salt and the interfacial interaction between the composite components. The intrinsic disordering of a conventional ionic crystal involves the stages of the defect formation in the bulk and on the surface of the crystal. The surface disordering is well described by the Stern model, which allows the surface potential to be easily calculated. The same model can be employed for the description of the mechanism of defect formation as the main stage of the interfacial interaction. Methods for the estimation of the conductivity and other physicochemical characteristics of composites were proposed. The problems of the thermodynamic stability of nanocomposites and the genesis of their morphology during the sintering were considered. The general peculiarities of the variation of ionic salt properties in a wide series of the ionic salt–oxide systems were analysed as well as the size effects.

In heterogeneous systems with sufficiently strong interfacial interaction, the effect of self-dispersion of an ionic salt was observed, which allowed the nanocomposites to be synthesised by the method of liquid-phase or solid-phase spreading. The nanosize state of a salt in systems thus obtained is thermodynamically stable if the size of oxide particles remains constant. Based on the combined studies of a wide series of composites MX–A with different ionic compounds, it was shown that nanocomposites are characterised by considerable changes in the thermodynamic and structural properties of ionic salts. These changes manifest themselves most clearly in compounds that contain high-temperature disordered phases, namely, AgI, $Li_2SO_4$ and alkali metal nitrates. Disordered crystalline surface phases are stabilised in silver iodide and lithium sulfate, whereas the amorphous state is stabilised in nitrates. Rapid quenching of nanocomposites $AgI-Al_2O_3$ allowed amorphous silver iodide to be obtained for the first time. This convincingly proves that the pronounced size effects can be observed on going from microsystems to nanoscale systems, which opens up the possibility for the synthesis of new materials with unusual properties.

I am grateful to my teachers, academician V V Boldyrev and Dr. E F Hairetdinov for their help and constant supervision and also to the scientists of the Institute of Solid State Chemistry and Mechanochemistry of the Siberian Branch of the Russian Academy of Sciences (Novosibirsk) V G Ponomareva, G V Lavrova, L I Brezhneva, V P Isupov, A A Politov, B B Bokhonov, A P Nemudry, V V Zyryanov, I I Gainutdinov, Yu T Pavlyukhin, Yu G Mateishina, A S Ulihin and others who took active part in carrying out experiments and their discussion. I would like to express my sincere gratitude to academician V M Bouznik, corresponding member of RAS Yu A Kotov and professors A Ya Neiman, Yu I Aristov, A K Ivanov-Shits, I V Murin and Yu M Baikov for fruitful discussions of different aspects of these studies; to foreign scientists W Bollmann (Gernamy), A K Shukla and K J Rao (India), J Maier (Germany), P Vaněk, J Petzelt (Czech Republic) and G Meng (China) for the possibility of carrying out joint studies within the frames of various International programmes and also to academician Yu D Tretyakov for the proposal to publish this review in the special issue of this journal.

## References


1. V N Chebotin, M V Perfil'ev *Elektrokhimiya Tverdykh Elektrolitov* (Electrochemistry of Solid Electrolytes) (Moscow: Khimiya, 1978)
2. E A Ukshe, N G Bukun *Tverdye Elektrolity* (Solid Electrolytes) (Moscow: Nauka, 1977)
3. A K Ivanov-Shits, I V Murin *Ionika Tverdogo Tela* (Solid State Ionics) Vol. 1 (St Petersburg: St Petersburg State University, 2000)
4. C C Liang *J. Electrochem. Soc.* **120** 1289 (1973)
5. C C Liang, A V Joshi, N E Hamilton *J. Appl. Electrochem.* **8** 445 (1978)
6. J Maier *J. Phys. Chem. Solids* **46** 309 (1985)
7. J B Wagner *NATO ASI Ser., Ser. E* **101** 77 (1985)
8. A K Shukla, N Vaidehi, K T Jacob *Proc. Indian Acad. Sci., Chem. Sci.* **96** 533 (1986)
9. J Maier *Ber. Bunsen-Ges. Phys. Chem.* **90** 26 (1986)
10. J Maier *J. Electrochem. Soc.* **134** 1524 (1987)
11. R Blender, W Dieterich *J. Phys. C* **20** 6113 (1987)
12. J B Wagner *High Conductivity Conductors: Solid Ionic Conductors* (Ed. T Takahashi) (Singapore: World Sci. Publ., 1989) p. 102
13. J Maier *Superionic Solids and Solid Electrolytes: Recent Trends* (Eds S Chandra, A Laskar) (New York: Academic Press, 1989) p. 137
14. N J Dudney *Annu. Rev. Mater. Sci.* **19** 103 (1989)
15. J Maier *Prog. Solid State Chem.* **23** 171 (1995)
16. R C Agrawal, R K Gupta *J. Mater. Sci.* **34** 1131 (1999)
17. I Kosacki, T Suzuki, V Petrovsky, H U Anderson *Solid State Ionics* **136 – 137** 1225 (2000)
18. A Yaroslavtsev *Russ. J. Inorg. Chem. (Suppl. 3)* **45** 249 (2000)
19. P Heitjans, S Indris *J. Phys.: Condens. Matter* **15** 1257 (2003)
20. J Schoonman *Solid State Ionics* **157** 319 (2003)
21. A B Yaroslavtsev, V V Nikonenko, V I Zabolotsky *Usp. Khim.* **72** 438 (2003) [*Russ. Chem. Rev.***72** 393 (2003)]
22. B S Bokshtein, A B Yaroslavtsev *Diffuziya Atomov i Ionov v Tverdykh Telakh* (Diffusion of Atoms and Ions in Solids) (Moscow: Moscow Institute of Steel and Melts, 2005)
23. Ya I Frenkel *Kineticheskaya Teoriya Zhidkostei* (Kinetic Theory of Liquids) (Moscow: Academy of Sciences of the USSR, 1945)
24. N F Uvarov, Doctoral Thesis in Chemical Sciences, Institute of Solid State Chemistry and Mechanochemistry, Siberian Branch of the Russian Academy of Sciences, Novosibirsk, 1998
25. P Chowdhary, V B Tare, J B Wagner *J. Electrochem. Soc.* **132** 123 (1985)
26. A C Khandkar, J B Wagner *Solid State Ionics* **18 – 19** 1100 (1986)
27. L Chen *Materials for Solid State Batteries* (Eds B V R Chowdari, S Radhakrishna) (Singapore: World Sci. Publ., 1986) p. 69
28. N F Uvarov, E F Hairetdinov, V V Boldyrev *J. Solid State Chem.* **51** 59 (1984)
29. N F Uvarov, E F Hairetdinov, V V Boldyrev *Izv. Sib. Otd. Akad. Nauk, Ser. Khim. Nauk* 1 (3) 3 (1984)
30. N F Uvarov, E F Hairetdinov, V V Boldyrev *Dokl. Akad. Nauk SSSR* **274** 661 (1984) [a]
31. N F Uvarov, E F Hairetdinov *J. Therm. Anal.* **33** 279 (1988)
32. N F Uvarov, W Bollmann, E F Hairetdinov *Cryst. Res. Technol.* **24** 413 (1989)
33. W Bollmann, N F Uvarov, E F Hairetdinov *Cryst. Res. Technol.* **24** 421 (1989)
34. N F Uvarov, E F Hairetdinov *Izv. Sib. Otd. Akad. Nauk, Ser. Khim. Nauk* 6 (17) 89 (1986)
35. N F Uvarov, W Bollmann, E F Hairetdinov *Cryst. Res. Technol.* **24** 543 (1989)
36. N F Uvarov, E F Hairetdinov *Izv. Sib. Otd. Akad. Nauk, Ser. Khim. Nauk* 3 (8) 6 (1984)
37. D J Fisher *Rules of Thumb for Physical Scientists* (Aedermannsdorf: Trans Tech Publ., 1988)
38. Yu Ya Gurevich *Dokl. Akad. Nauk SSSR* **222** 143 (1975) [a]
39. Yu Ya Gurevich, Yu I Kharkats *Zh. Eksp. Teor. Fiz.* **72** 1845 (1977) [b]
40. Yu Ya Gurevich, Yu I Kharkats *Khimiya Tverdogo Tela (Itogi Nauki i Tekhniki)* [Solid State Chemistry (Advances in Science and Engineering Series)] (Moscow: Izd. VINITI, 1987) Vol. 4, p. 3
41. A Lunden *Solid State Commun.* **65** 1237 (1988)
42. N F Uvarov, E F Hairetdinov, V V Boldyrev *Izv. Sib. Otd. Akad. Nauk, Ser. Khim. Nauk* 6 (14) 27 (1981)
43. N Parsonage, L Staveley *Disorder in Crystals* (Oxford: Oxford University Press, 1978)
44. N F Uvarov, I A Gonysheva *Tezisy Dokladov IV Ural'skoi Konferentsii po Vysokotemperaturnoi Fizicheskoi Khimii i Elektrokhimii, Perm', 1985* (Abstracts of Reports of the IVth Urals Conference on High-Temperature Physical Chemistry and Electrochemistry, Perm, 1985) p. 126
45. K Lehovec *J. Chem. Phys.* **21** 1123 (1953)
46. F Kröger *The Chemistry of Imperfect Crystals* (Amsterdam: North-Holland, 1964)
47. K L Kliewer, K S Koehler *Phys. Rev., Sect. A* **140** 1226 (1965)
48. K L Kliewer *J. Phys. Chem. Solids* **27** 705 (1966)
49. O Stern *Z. Electrochem.* **30** 508 (1924)
50. N F Uvarov *Elektrokhimiya* (2007) (in the press) [c]
51. I M Lifshits, Ya E Geguzin *Fiz. Tv. Tela* **7** (1) 62 (1965) [d]
52. R B Poeppel, J M Blakely *Surf. Sci.* **15** 507 (1969)
53. N F Uvarov, V P Isupov, V Sharma, A K Shukla *Solid State Ionics* **51** 41 (1992)
54. N F Uvarov, E F Hairetdinov *Solid State Ionics* **96** 219 (1997)
55. N F Uvarov, E F Hairetdinov *Solid State Ionics* **96** 227 (1997)
56. N F Uvarov, E F Hairetdinov, A I Rykov, Yu T Pavlyukhin *Solid State Ionics* **96** 233 (1997)
57. N F Uvarov, A K Tsvetnikov, V M Bouznik *Tezisy Dokladov XII Rossiiskoi Konferentsii po Fizicheskoi Khimii i Elektrokhimii Rasplavlennykh i Tverdykh Elektrolitov, Nal'chik, 2001* [Abstracts of Reports of the XIIth Russian Conference on Physical Chemistry and Electrochemistry of Molten and Solid Electrolytes, Nal'chik, 2001] Vol. 2, p. 111
58. *Metallopolimernye Nanokompozity (Poluchenie, Svoistva, Primenenie) (Integratsionnye Proekty SO RAN)* [Metal-polymeric Nanocomposites (Production, Properties and Applications) (Integration Projects of Siberian Branch of the Russian Academy of Sciences)] (Novosibirsk: Siberian Branch of the Russion Academy of Sciences, 2005) No. 2
59. A K Shukla, R Manoharan, J B Goodenough *Solid State Ionics* **26** 5 (1988)
60. N F Uvarov, V G Ponomareva *Dokl. Akad. Nauk* **351** 358 (1996) [a]
61. N F Uvarov, E F Hairetdinov, B B Bokhonov, N B Bratel *Solid State Ionics* **86 – 88** 573 (1996)
62. B Zhu, B-E Mellander *Solid State Ionics* **77** 244 (1995)
63. B Zhu, B-E Mellander *Solid State Ionics* **70 – 71** 285 (1994)
64. N F Uvarov, J Maier *Solid State Ionics* **62** 251 (1993)
65. N F Uvarov, E F Hairetdinov *J. Solid State Chem.* **62** 1 (1986)
66. N F Uvarov, E F Hairetdinov *Izv. Sib. Otd. Akad. Nauk, Ser. Khim. Nauk* 2 (5) 43 (1985)
67. N F Uvarov, P Vaněk, Yu I Yuzyuk, V ŽeleznyZh, V Studnička, B B Bokhonov, V E Dulepov, J Petzelt *Solid State Ionics* **90** 201 (1996)
68. N F Uvarov *Dokl. Akad Nauk* **353** 213 (1997) [a]
69. N F Uvarov *Solid State Ionics* **136 – 137** 1267 (2000)
70. D S McLachlan, M Blaszkiewicz, R E Newnham *J. Am. Ceram. Soc.* **73** 2187 (1990)
71. N F Uvarov, E F Hairetdinov, N B Bratel *Elektrokhimiya* **29** 1406 (1993) [c]
72. A M Stoneham, E Wade, J A Kilner *Mater. Res. Bull.* **14** 661 (1979)
73. N J Dudney *J. Am. Ceram. Soc.* **68** 538 (1985)
74. J C Wang, N J Dudney *Solid State Ionics* **18 – 19** 112 (1986)
75. H E Roman, A Bunde, W Dieterich *Phys. Rev. B* **34** 3439 (1986)
76. H E Roman, M Yusouff *Phys. Rev. B* **36** 7285 (1987)
77. H E Roman *J. Phys.: Condens. Matter* **2** 3909 (1990)
78. C W Nan, D M Smith *Mater. Sci. Eng., B* **10** 99 (1991)
79. M Siekierski, J Przyluski *Proceedings of the 4th Asian Conference on Solid State Ionics* (Singapore: World Sci. Publ., 1994) p. 121

80. S Jiang, J B Wagner Jr *J. Phys. Chem. Solids* **56** 1113 (1995)
81. Mikrajuddin, F G Shi, K Okuyama *J. Electrochem. Soc.* **147** 3157 (2000)
82. N F Uvarov, B B Bokhonov, V P Isupov, E F Hairetdinov *Solid State Ionics* **74** 15 (1994)
83. N F Uvarov, B B Bokhonov, V P Isupov, E F Hairetdinov *Yavleniya Elektroperenosa v Oksidnykh Sistemakh* (Effects of Electricity Transfer in Oxide Systems) (Ekaterinburg: Institute of High-temperature Electrochemistry, Urals Branch of the Russian Academy of Sciences, 1994) p. 45
84. N F Uvarov, V V Boldyrev *Usp. Khim.* **70** 307 (2001) [*Russ. Chem. Rev.* **70** 265 (2001)]
85. B Ya Pines *Ocherki o Metallofizike* (Essays on Physics of Metals) (Kharkov: Kharkov University, 1961)
86. Ya E Geguzin *Fizika Spekaniya* (The Physics of Agglomeration) (Moscow: Nauka, 1984)
87. P W Tasker *Philos. Mag. A* **39** 119 (1979)
88. V L Tauson, M G Abramovich *Fiziko-khimicheskie Prevrashcheniya Real'nykh Kristallov v Mineral'nykh Sistemakh* (Physicochemical Transformations of Real Crystals in Mineral Systems) (Novosibirsk: Nauka, 1988)
89. A Adamson *The Physical Chemistry of Surfaces* (New York: Wiley, 1976)
90. N F Uvarov, M C R Shastry, K J Rao *Rev. Solid State Sci.* **4** 61 (1990)
91. N F Uvarov, B B Bokhonov, A A Politov, P Vaněk, J Petzelt *J. Mater. Synth. Process.* **8** 327 (2000)
92. N F Uvarov, P Vaněk, M Savinov, V ŽeleznyZh, J Studnička, J Petzelt *Solid State Ionics* **127** 253 (2000)
93. N F Uvarov, O P Shrivastava, E F Hairetdinov *Solid State Ionics* **36** 39 (1989)
94. N F Uvarov, O P Srivastava, E F Hairetdinov *Proc. Indian Natl. Sci. Acad., Part A* **55** 703 (1989)
95. N F Uvarov, E F Hairetdinov, I V Skobelev *Solid State Ionics* **86**–**88** 577 (1996)
96. N F Uvarov, I V Skobelev, B B Bokhonov, E F Hairetdinov *J. Mater. Synth. Process.* **4** 391 (1996)
97. N F Uvarov *The International Symposium on Metastable, Mechanically Alloyed and Nanocrystalline Materials (Abstracts of Papers), Ann Arbor, MI, 2001* p. 27
98. L S Palatnik, I I Papirov *Epitaksial'nye Plenki* (Epitaxial Films) (Moscow: Nauka, 1971)
99. I D Morokhov, L I Trusov, S P Chizhik *Ul'tradispersnye Metallicheskie Sredy* (Ultradispersed Metallic Media) (Moscow: Atomizdat, 1977)
100. Yu F Komnik *Fizika Metallicheskikh Plenok. Razmernye i Strukturnye Effekty* (The Physics of Metallic Films. Size and Structure Effects) (Moscow: Atomizdat, 1979)
101. S A Nepiiko *Fizicheskie Svoistva Malykh Metallicheskikh Chastits* (Physical Properties of Small Metallic Particles) (Kiev: Naukova Dumka, 1985)
102. Yu I Petrov *Klastery i Malye Chastitsy* (Clusters and Small Particles) (Moscow: Nauka, 1986)
103. H Gleiter *Prog. Mater. Sci.* **33** 223 (1989)
104. H Gleiter *J. Appl. Crystallogr.* **24** 79 (1991)
105. V G Gryaznov, L I Trusov *Prog. Mater. Sci.* **37** 289 (1993)
106. Yu I Vesnin *Vtorichnaya Struktura i Svoistva Kristallov* (Secondary Structure and Properties of Crystals) (Novosibirsk: Institute of Inorganic Chemistry of Siberian Branch of the Russian Academy of Sciences, 1997)
107. R F Khairutdinov *Usp. Khim.* **67** 125 (1998) [*Russ. Chem. Rev.* **67** 109 (1998)]
108. A I Gusev *Nanokristallicheskie Materialy: Metody Polucheniya i Svoistva* (Nanocrystalline Materials: Methods of Production and Properties) (Ekaterinburg: Urals Branch of Russian Academy of Sciences, 1998)
109. D G Morris *Mechanical Behaviour of Nanostructured Materials (Materials Science Foundations)* (Zuerich: Trans Tech Publ., 1998) Vol. 2
110. R A Andrievskii, A M Glezer *Fiz. Met. Metalloved.* **88** 50 (1999) [e]
111. A I Gusev, A A Rempel *Nanokristallicheskie Materialy* (Nanocrystalline Materials) (Moscow: Fizmatlit, 2000)
112. R Z Valiev, I V Aleksandrov *Nanostrukturnye Materialy, Poluchennye Intensivnoi Plasticheskoi Deformatsiei* (Nanostructural Materials, Production by Intensive Plastic Deformation) (Moscow: Logos, 2000)
113. H Gleiter *Acta Mater.* **48** 1 (2000)
114. *Zernogranichnaya Diffuziya i Svoistva Nanostrukturnykh Materialov* (Grain-boundary Diffusion and Properties of Nanostructural Materials) (Eds Yu R Kolobov, R Z Valiev) (Novosibirsk: Nauka, 2001)
115. R A Andrievskii *Usp. Khim.* **71** 967 (2002) [*Russ. Chem. Rev.* **71** 853 (2002)]
116. V Ya Shevchenko, A E Madison *Fiz. Khim. Stekla* **28** 60 (2002) [f]
117. V Ya Shevchenko, A E Madison *Fiz. Khim. Stekla* **28** 65 (2002) [f]
118. J Maier *Solid State Ionics* **148** 367 (2002)
119. J Maier *Solid State Ionics* **154**–**155** 291 (2002)
120. G B Sergeev *Nanokhimiya* (Nanochemistry) (Moscow: Moscow State University, 2003)
121. Yu D Tretyakov *Usp. Khim.* **72** 731 (2003) [*Russ. Chem. Rev.* **72** 651 (2003)]
122. V I Roldugin *Usp. Khim.* **73** 123 (2004) [*Russ. Chem. Rev.* **73** 115 (2004)]
123. L I Grechikhin *Fizika Nanochastits i Nanotekhnologii. Obshchie Osnovy, Mekhanicheskie, Teplovye i Emissionnye Svoistva* (The Physics of Nanoparticles and Nanotechnologies. General Foundations, Mechanical, Thermal and Emission Properties (Minsk: Tekhnoprint, 2004)
124. P Buler *Nanotermodinamika* (Nanothermodynamics) (St Petersburg: Yanus, 2004)
125. F Kh Urakaev, V V Boldyrev *Zh. Fiz. Khim.* **79** 662 (2005) [g]
126. I P Suzdalev *Nanotekhnologiya: Fiziko-khimiya Nanoklasterov, Nanostruktur i Nanomaterialov* (Nanotechnology: Physicochemistry of Nanoclusters, Nanostructures and Nanomaterials) (Moscow: KomKniga, 2005)
127. A I Gusev *Nanomaterialy, Nanostruktury, Nanotekhnologii* (Nanomaterials, Nanostructures and Nanotechnologies) (Moscow: Fizmatlit, 2005)
128. A L Despotuli, A V Andreeva, B Rambabu *Nano Mikrosistem. Tekh.* (2) 5 (2005)
129. L M Shcherbakov *Issledovaniya v Oblasti Poverkhnostnykh Sil* (Investigation in the Field of Surface Forces) (Moscow: Academy of Sciences of the USSR, 1961) p. 28
130. L M Shcherbakov *Poverkhnostnye Yavleniya v Rasplavakh i Voznikayushchikh iz Nikh Tverdykh Fazakh* (Surface Effects in Melts and Solid Phases Formed in Them) (Kishinev: Shtiintsa, 1974) p. 76
131. L S Palatnik, M Ya Fuks, V M Kosevich *Mekhanizm Obrazovaniya i Substruktura Kondensirovannykh Plenok* (The Mechanism of Formation and Substructure of Condensed Films) (Moscow: Nauka, 1972)
132. W A Jesser, D Kulmann-Wilsdorf *Phys. Status Solidi* **19** 95 (1967)
133. Yu G Sidorov, E M Trukhanov *Poverkhnost'* **6** 106 (1992)
134. N F Uvarov *Izv. Bolg. Akad. Nauk, Khim.* **23** 619 (1990)
135. E F Hairetdinov, N F Uvarov *Mater. Sci. Forum* **88**–**90** 723 (1992)
136. N F Uvarov, E F Hairetdinov *Solid State Phenomena* **39**–**40** 27 (1994)
137. N F Uvarov, V G Ponomareva, G V Lavrova, N B Bratel', I V Skobelev, E F Hairetdinov *Fundamental'nye Issledovaniya Novykh Materialov i Protsessov v Veshchestve* (Fundamental Investigations of New Materials and Processes in Substance) (Eds A N Tikhonov, V A Sadovnichii) (Moscow: Moscow State University, 1994) Vol. 1, p. 70
138. N F Uvarov *Solid State Ionics: New Developments.* (Eds B V R Chowdary, M A K L Dissanayake, M A Careem) (Singapore: World Sci. Publ., 1996) p. 311
139. N F Uvarov *Zh. Prikl. Khim.* **73** 970 (2000) [h]
140. N F Uvarov, A A Politov, B B Bokhonov *Solid State Ionics: Materials and Devices* (Eds B V R Chowdary, W Wang) (Singapore: World Sci. Publ., 2000) p. 113
141. N F Uvarov, P Vaněk *J. Mater. Synth. Process.* **8** 319 (2000)
142. N F Uvarov, V G Ponomareva, G V Lavrova, L I Brezhneva *Mater. Sci. Forum* **386**–**387** 639 (2002)

143. N F Uvarov, V G Ponomareva *Nanotechnologies in the Area of Physics, Chemistry and Biotechnology. Fifth ISTC SAC Seminar, St Petersburg, 2002* p. 53
144. N F Uvarov, L I Brezhneva, E F Hairetdinov *Solid State Ionics* **136–137** 1273 (2000)
145. G V Lavrova, V G Ponomareva, N F Uvarov *Solid State Ionics* **136–137** 1285 (2000)
146. V G Ponomareva, G V Lavrova, N F Uvarov, E F Hairetdinov *Solid State Ionics* **90** 161 (1996)
147. V G Ponomareva, G V Lavrova, N F Uvarov *Solid State Ionics: New Developments* (Eds B V R Chowdary, M A K L Dissanayake, M A Careem) (Singapore: World Sci. Publ., 1996) p. 317
148. A S Ulihin, N F Uvarov, Yu G Mateyshina, L I Brezhneva, A A Matvienko *Solid State Ionics* **177** 2787 (2006)
149. A Ya Neiman, N F Uvarov, N N Pestereva *Solid State Ionics* **177** 3361 (2007)
150. V V Boldyrev *Eksperimental'nye Metody v Mekhanokhimii Tverdykh Neorganicheskikh Veshchestv* (Experimental Methods in Mechanochemistry of Inorganic Solids) (Novosibirsk: Nauka, 1983)
151. V A Pavlov *Fiz. Met. Metalloved.* **59** 629 (1985) [e]
152. W L Johnson *Prog. Mater Sci.* **30** 81 (1986)
153. E G Avvakumov *Mekhanicheskie Metody Aktivatsii Khimicheskikh Protsessov* (Mechanical Methods of Activation of Chemical Processes) (Novosibirsk: Nauka, 1986)
154. C C Koch *Annu. Rev. Mater. Sci.* **19** 123 (1989)
155. A V Serebryakov *Metallofizika* **13** (5) 115 (1991)
156. *Mekhanokhimicheskii Sintez v Neorganicheskoi Khimii* (Mechanochemical Synthesis in Inorganic Chemistry) (Ed. E G Avvakumov) (Novosibirsk: Nauka, 1991)
157. *Mechanical Alloying (Mater. Sci. Forum.)* Vols 88–90 (Ed. P H Shingu) (Zuerich: Trans Tech Publ., 1992)
158. P Yu Butyagin *Usp. Khim.* **63** 1031 (1994) [*Russ. Chem. Rev.* **63** 965 (1994)]
159. V A Gusev, V A Gagarina, E M Moroz, E A Levitskii *Kristallografiya* **19** 1289 (1974) [i]
160. V A Gusev, V A Gagarina, E M Moroz, E A Levitskii *Kinet. Katal.* **17** 500 (1976) [j]
161. Yu I Aristov, M M Tokarev, G Cacciola, G Restuccia *React. Kinet. Catal. Lett.* **59** 325 (1996)
162. Yu I Aristov, M M Tokarev, G Di Marko, G Kachchiola, D Restuchcha, V N Parmon *Zh. Fiz. Khim.* **71** 253 (1997) [g]
163. L G Gordeeva, D Restuchcha, G Kachchiola, Yu I Aristov *Zh. Fiz. Khim.* **72** 1236 (1998) [g]
164. L G Gordeeva, Candidate Thesis in Chemical Sciences, Institute of Catalysis, Siberian Branch of Russian Academy of Sciences, Novosibirsk, 1998
165. L G Gordeeva, G Restuccia, A Freni, Yu I Aristov *Fuel Process. Technol.* **79** 225 (2002)
166. L G Gordeeva, I S Glaznev, Yu I Aristov *Zh. Fiz. Khim.* **77** 1906 (2003) [g]
167. L G Gordeeva, I S Glaznev, V V Malakhov, Yu I Aristov *Zh. Fiz. Khim.* **77** 2048 (2003) [g]
168. R W J M Huang Foen Chung, S W de Leeuw *Solid State Ionics* **175** 851 (2004)
169. I I Gainutdinov, N F Uvarov *Solid State Ionics* **177** 1631 (2006)
170. V G Ponomareva, G V Lavrova, L G Simonova *Solid State Ionics* **118** 317 (1999)
171. V G Ponomareva, G V Lavrova *Solid State Ionics* **145** 197 (2001)
172. G V Lavrova, V G Ponomareva *Neorg. Mater.* **38** 1386 (2002) [k]
173. V G Ponomareva, G V Lavrova, E B Burgina *Solid State Ionics* **176** 767 (2005)
174. V G Ponomareva, B V Merinov, G V Lavrova *Solid State Ionics* **145** 205 (2001)
175. V G Ponomareva, E S Shutova, A A Matvienko *Neorg. Mater.* **40** 721 (2004) [k]
176. V G Ponomareva, E S Shutova *Solid State Ionics* **176** 2905 (2005)
177. E Konisheva, A Neiman, E Gorbunova *Solid State Ionics* **157** 45 (2003)
178. A Ya Neiman, N N Pestereva, A R Sharafutdinov, Yu P Kostikov *Elektrokhimiya* **41** 680 (2005) [c]
179. N Sata, K Ebermann, K Eberl, J Maier *Nature (London)* **408** 946 (2000)
180. N Y Jin-Phillipp, N Sata, J Maier, C Scheu, K Hahn, M Kelsch, M Ruhle *J. Chem. Phys.* **120** 2375 (2004)
181. A Nemudry, P Rudolf, R Schöllhorn *Chem. Mater.* **8** 2232 (1996)
182. A Nemudry, E L Goldberg, M Aguirre, M Á Alario-Franco *Solid State Sci.* **4** 677 (2002)
183. N F Uvarov, A P Nemudry *Proceedings of the Xth APAM Topical Seminar 'Nanoscience and Technology', Novosibirsk, 2003* p. 56
184. J M Reau, P Hagenmuller *Appl. Phys. A* **49** 3 (1989)
185. G V Lavrova, M V Russkikh, V G Ponomareva, N F Uvarov *Elektrokhimiya* **41** 556 (2005) [c]
186. G V Lavrova, M V Russkih, V G Ponomareva, N F Uvarov *Solid State Ionics* **177** 2129 (2006)
187. S M Haile, D A Boysen, C R I Chisholm, R B Merle *Nature (London)* **410** 910 (2001)
188. Yu G Mateyshina, N F Uvarov, A S Ulihin, Yu T Pavlyuhin *Solid State Ionics* **177** 2769 (2006)

[a] — *Dokl. Chem. (Engl. Transl.)*
[b] — *J. Exp. Theor. Phys. (Engl. Transl.)*
[c] — *Russ. J. Electrochem. (Engl. Transl.)*
[d] — *Phys. Solid State (Engl. Transl.)*
[e] — *Phys. Met. Metallogr. (Engl. Transl.)*
[f] — *Glass Phys. Chem. (Engl. Transl.)*
[g] — *Russ. J. Phys. Chem. (Engl. Transl.)*
[h] — *Russ. J. Appl. Chem. (Engl. Transl.)*
[i] — *Crystallogr. Rep. (Engl. Transl.)*
[j] — *Kinet. Catal. (Engl. Transl.)*
[k] — *Inorg. Mater. (Engl. Transl.)*